Petroleum Science 23 (2026) 278–296

Contents lists available at ScienceDirect

Petroleum Science

journal homepage: www.keaipublishing.com/en/journals/petroleum-science

Original Paper

Development of mahua oil (*Madhuca indica*) methyl ester based drilling mud as a sustainable alternative to oil based mud for unconventional reservoirs

Bhola Kumar Paswan [a], Smruti Naik [b], Puja Hansdah [c], Sidharth Gautam [d,*]

[a] Department of Petroleum Engineering, Parul University, Vadodara, Gujarat, India
[b] Department of Chemical Engineering, Indian Institute of Technology, Delhi, India
[c] Department of Mining Engineering, O. P. Jindal University, Raigarh, Chattisgarh, India
[d] Department of Petroleum Engineering and Geoengineering, Rajiv Gandhi Institute of Petroleum Technology, Jais, Amethi, India

ARTICLE INFO

Article history:
Received 6 March 2025
Received in revised form
12 October 2025
Accepted 11 December 2025
Available online 17 December 2025

Edited by Jia-Jia Fei

Keywords:
Drilling fluid
Methyl ester
Oil in water emulsion
Rheology
Shale inhibition

ABSTRACT

The exploration of untapped unconventional reservoirs has increased to fulfill the growing global demand for energy. Traditionally, oil-based mud (OBM) is preferred for drilling such formations; however, it has shortcomings such as environmental concerns, high cost, complex handling and disposal, and logistical challenges. In this regard, vegetable oil derivatives offer a viable alternative, addressing the shortcomings of OBMs while maintaining performance. In this study, mahua oil methyl ester (MME) is synthesized from mahua oil (*Madhuca indica*) through a transesterification reaction. The synthesized MME is used as a dispersed phase to formulate an oil-in-water (O/W) emulsion mud (MME mud). The rheological, filtration, and shale inhibition capabilities of the formulated MME mud are compared with those of the conventional diesel oil-based mud (diesel mud). The MME mud offered an improved performance with an 18% increase in rheological properties and a 40% reduction in filtration loss volume as compared to diesel mud. The developed MME mud also demonstrated excellent tolerance towards salt contamination and enhanced lubricity compared to diesel-based mud. The viscoelastic studies of the MME mud showed the dominance of elastic modulus over viscous modulus, indicating the structural stability of the O/W emulsion mud. Additionally, the frequency sweep test revealed the mud to behave as a viscoelastic solid under both fast and slow deformation, which is essential for suspending drill cuttings during drilling and periods of low or no flow. The interaction of formulated mud with drill cutting was evaluated by the shale dispersion and slake durability tests. The primary shale recovery of the MME mud was 91.5%, indicating a benign and non-interacting nature of MME mud. Similarly, the slake durability index of MME mud was 86.15%, indicating outstanding inhibitive properties in MME mud. The environmental assessment of MME revealed the absence of aromatic components and a higher LC_{50}, indicating better biodegradability and lower toxicity compared to diesel. The findings of the study indicate that MME mud offers improved drilling performance, environmental compliance, and economic benefits, positioning it as a sustainable alternative to diesel oil-based mud and making it possible for application in drilling unconventional reservoirs.

1. Introduction

The petroleum industry is under pressure to find untapped potential in deep and unconventional regions due to the ongoing decrease of shallow fossil fuel assets and rising energy needs (Bayat et al., 2021). These reservoirs frequently experience challenging circumstances, such as high temperature or pressure, and shale-related problems, such as sloughing, swelling, and dispersion, demanding improved technologies and careful drilling strategies (Adams and Charrier, 1985). So, for a competitive and cost-effective drilling process, it is crucial to develop drilling mud for drilling unconventional reservoirs. The drilling fluid, also called

* Corresponding author.
E-mail address: sidharth@rgipt.ac.in (S. Gautam).
Peer review under the responsibility of China University of Petroleum (Beijing).

https://doi.org/10.1016/j.petsci.2025.12.019

drilling mud, is a central part of the drilling process. Its primary functions include lifting drilling cuttings and solids from the wellbore floor to the surface and keeping them suspended during breakdowns to prevent precipitation (Saleh and Ibrahim, 2019). Additionally, the drilling mud controls the formation pressure to stop the fluid influx into the borehole during drilling and preserves wellbore stability while lubricating and cooling the drill bit (Abdo and Haneef, 2012). Based on the features of the lithologies, the choice of drilling fluid is made to maximize the drilling process. Therefore, effective fluid choice is essential for smooth drilling and completion processes (Fakoya and Ahmed, 2018). A poor choice of drilling fluid can result in several drilling issues, such as wellbore instability, pipe sticking, clay swelling, lost circulation, and shale sloughing (Abdo and Haneef, 2012; Saleh and Ibrahim, 2019). Drilling muds are typically categorized into three primary types: water-based muds (WBM), oil-based muds (OBM), and synthetic-based muds (SBM). Water-based mud (WBM) is the most utilized drilling fluid in the drilling process. It is cost-effective, environmentally acceptable, and recommended for low-pressure, low-temperature drilling processes (Edalatfar et al., 2021). However, OBM is preferred for its exceptional ability to drill difficult high-pressure and high-temperature (HPHT) wells. OBM offers excellent shale stabilization, contaminant resistance, higher temperature stability, and faster penetration rates (Cheraghian, 2017). Moreover, compared to WBMs, the characteristics of OBMs do not significantly alter upon physical contact with the formation fluid (Fakoya and Ahmed, 2018).

Several authors reported that 423.7 tonnes (on average) of cuttings are typically brought to the surface after drilling a conventional well (Melton et al., 2000; Sulaimon et al., 2017). OBMs can often be poisonous and pollute these cuttings, making them hazardous to the environment. Therefore, before being disposed of, drill cuttings need to be treated, which increases the drilling cost significantly. Further, conventional diesel oil contains 10%–30% aromatics, making it non-biodegradable and prone to bioaccumulate (Sulaimon et al., 2017). Due to its environmental shortcomings, diesel is being replaced with more environmentally friendly alternatives such as white synthetic oils. However, it still finds significant use in onshore drilling operations, especially in challenging geological formations such as unconventional shale and HPHT reservoirs (Baxter et al., 2018). Its cost-effectiveness makes it a preferred choice for drilling cost-sensitive locations (Tiwari et al., 2020). Despite several environmental concerns, diesel oil continues to be widely used in drilling operations, making it a critical area of research to develop ecologically acceptable and economically viable alternatives.

As a potential substitute for traditional mineral/diesel oils, vegetable oils are affordable, easily accessible, and environmentally benign (Sulaimon et al., 2017). In this regard, several authors have studied the possible utilization of vegetable oils to formulate environmentally friendly drilling fluids (Amanullah, 2005; Razali et al., 2018). Vegetable oils, such as castor oil (Setyawan, 2018), soybean oil (Ratkievicius et al., 2017), groundnut oil (Adewale and Ogunrinde, 2010), and rapeseed oil (Lysakova et al., 2025), have been directly utilized as a replacement for diesel or mineral oil in a typical drilling fluid formulation. Although vegetable oil may be directly used for drilling fluid formulation, it poses challenges like (a) degradation at high temperatures, (b) oxidation and rancidification over time, and (c) incompatibility with existing drilling fluid additives (Fox and Stachowiak, 2007). Additionally, typical vegetable oil may have a viscosity 4–5 times higher than diesel oil, thus violating the ASTM specification D975 (ASTM D975, 2021), which mandates a diesel viscosity of 1.3–4.1 cSt. Consequently, the high viscosity of the base fluid can cause undesirable rheological characteristics, resulting in reduced penetration rate, increased swab and surge pressure, differential sticking, high pumping pressure to initiate flow, and high equivalent circulating density, which may result in formation fracture and lost circulation (Aboulrous et al., 2022). Thus, vegetable oils are inappropriate for application in synthetic base mud (Adewale and Ogunrinde, 2010).

Considering the essential properties of vegetable oil, such as affordability, accessibility, and an environmentally benign nature, it is necessary to modify vegetable oil to address the above-mentioned challenges and utilize it as an additive for drilling applications. This can be achieved by converting raw vegetable oil into an associated methyl ester via esterification and transesterification reactions (Sulaimon et al., 2017). The process consists of converting vegetable oil (triglycerides) into fatty acid methyl ester by reacting it with alcohol in the presence of a catalyst. The process reduces the viscosity and improves the biodegradability of formulated drilling fluids (Arain et al., 2022). Several studies have recently been conducted to utilize vegetable oil-derived methyl ester as an alternative to conventional diesel oil. The details of recent studies involving the conversion of raw vegetable oil into associated methyl ester and utilization in drilling fluid are presented in Table 1.

In this study, mahua oil (obtained from the seed kernel of *Madhuca indica*) with a fatty acid profile of palmitic acid, stearic acid, oleic acid, and linoleic acid is used as a vegetable oil for the preparation of the corresponding methyl ester (mahua oil methyl ester: MME) through transesterification reaction (Singh and Singh, 1991). Mahua is a native, biodegradable, and abundantly available plant. Additionally, the high flash point and fire point of mahua oil and its derivatives make it less dangerous to store and transport (Sharma Dugala et al., 2021), therefore avoiding the risk of fire hazards typically encountered with diesel oil. Thus, making it a suitable choice for exploring as an alternative to diesel in the formulation of oil-in-water (O/W) emulsion-based drilling mud. The O/W emulsion mud is preferred in this study over a more conventional invert emulsion (W/O) based mud due to the following inherited advantages such as (a) improved hole cleaning efficiency, (b) environmental friendliness and regulatory compliance (Liu et al., 2020), (c) lower cost (Paswan and Mahto, 2020), and (d) reduced risk of formation damage (Yue and Ma, 2008).

Over the years, the development of environmentally friendly alternatives to OBMs has received significant interest. However, existing studies have largely focused on empirical performance evaluation, with limited exploration of the molecular-level structure-performance relationships that govern drilling fluid behavior. The present study attempts to address this gap by systematically investigating the impact of the MME on the key performance characteristics of drilling fluid and linking them with the characteristics and molecular structure of MME. Therefore, the novelty of the present study is (a) formulation of MME-based O/W emulsion mud and evaluation of the mud performance parameters under both ambient and simulated downhole conditions, (b) a detailed comparative assessment with conventional diesel-based mud systems, including compatibility with additives, thermal stability, salt tolerance, lubricity, cuttings transport, formation damage, and shale inhibition, and (c) to establish a direct structure-performance relationships by linking the molecular structure and characteristics of MME to the enhanced drilling fluid properties. To the best of our knowledge, the mechanistic insight of the structure-performance relationship is not available in prior literature and represents a significant step toward the rational design of sustainable and high-performance drilling fluids involving vegetable oil-based methyl ester. The methodology adopted in this study is presented in Fig. 1.

Table 1
Utilization of vegetable oil-based derivatives for drilling fluid formulation.

Vegetable oil	Method	Mud type	Drilling fluid properties	Salient features	Reference
Palm oil	Interesterification	Invert emulsion mud	PV: 52 cP; YP: 5.76 Pa; 10 m GS: 4.79 Pa; MW: 8.28 ppg.	The formulated mud showed stable rheology up to a mud weight of 9.58 ppg.	Udoh et al. (2012)
Soybean oil	Soxhlet extraction	Invert emulsion mud	AV: 19 cP; PV: 11 cP; YP: 14 lb/100 ft^2; GS (10 s/10 m): 5/6 lb/100 ft^2; FL: 23 mL	The formed mud cake was thin and soft, making it suitable for averting stuck pipe situations.	Agwu et al. (2015)
Waste cooking oil	Transesterification	Invert emulsion mud	AV: 39.5 cP; PV: 29.0 cP; YP: 10.5 Pa; GS (10 s/10 m): 10/11 lb/100 ft^2; FL: 4 mL; ES: 2000 V	The formulated mud was non-toxic and exhibited excellent lubricity, making it suitable for extended-reach or directional wells.	Li et al. (2016b)
Palm oil	Transesterification	Invert emulsion mud	AV: 58.5 cP; PV: 30 cP; YP: 17 lb/100 ft^2; GS (10 s/10 m): 16/22 lb/100 ft^2; ES: 1600 mV	The mud showed a flat rheological profile and was found to be stable up to 120 °C and 10,000 psi.	Said and El-Sayed (2018)
Mango seed oil	Transesterification	Oil-in-water emulsion mud	AV: 26 cP; PV: 19 cP; YP: 14 lb/100 ft^2; GS (10 s/10 m): 3/4 lb/100 ft^2; FL: 3.0 mL	The mud showed high-temperature stability with constant viscosity up to 120 °C.	Kumar et al. (2020b)
Sunflower oil	Transesterification	Oil-in-water emulsion mud	AV: 25.5 cP; PV: 15 cP; YP: 21 lb/100 ft^2; GS (10 s/10 m): 3.0/5.5 lb/100 ft^2; FL: 8.0 mL	The mud showed high-temperature stability up to 140 °C.	Paswan and Mahto (2020)
Neem seed oil	Transesterification	Invert emulsion mud	PV: 15 cP; YP: 25 lb/100 ft^2; FL: 8.0 mL; MW: 8.05 ppg; CoF: 0.1768	The formulated methyl ester showed enhanced compatibility with OBM additives.	Fadairo et al. (2021)
Soybean oil	Transesterification	Invert emulsion mud	PV: 39 cP; YP: 9.2 Pa; GS (10 s/10 m): 3.5/4.0 Pa; FL: 1.4 mL	The mud showed temperature tolerance up to 160 °C and seawater tolerance up to 5%.	Jiang et al. (2022)
Calophyllum inophyllum	Two steps-Esterification and Transesterification	Invert emulsion mud	PV: 32 cP; YP: 6 lb/100 ft^2; FL: 3.6 mL; MW: 10.0 ppg; ES: 1475 V	The methyl ester has low kinematic viscosity and high flash point, making it suitable for forming a stable emulsion.	Arain et al. (2022)
Castor oil	Transesterification	Invert emulsion mud	PV: 34 cP; YP: 8 lb/100 ft^2; GS (10s/10 m): 7/9 lb/100 ft^2; FL: 3.2 mL; ES: 1232 V	The mud exhibits a fragile gel structure, facilitating efficient cutting and transport.	Arain et al. (2023)
Black seed oil (*Nigella Sativa L.*)	Transesterification	Invert emulsion mud	MW: 10 ppg; AV: 46.5 cP; PV: 41 cP; YP: 11 lb/100 ft^2; GS (10 s/10 m): 10/12 lb/100 ft^2	The formulated mud has a less harmful effect on plant growth.	Olaniyan and Sarah (2024)

AV: apparent viscosity; PV: plastic viscosity; YP: yield point; GS: gel strength; MW: mud weight; ES: electronic stability; FL: fluid loss volume.

2. Materials and methods

2.1. Materials

Raw mahua oil (color: dark yellow; density: 0.914 g·cm^{-3}; kinematic viscosity at 40 °C: 26.8 cSt) was procured from a local oil mill (Siwan, Bihar, India). Methanol (99.5%) is employed in the reactions, while KOH (in pellet form), which is used as a base catalyst and has a 99.5% purity level, is also used in the reactions. Xanthan gum (XG: molecular weight, 1.1 × 10^6 Da) and carboxy methyl cellulose (CMC: molecular weight, 2.6 × 10^5 Da; degree of substitution of carboxylic group: 0.51) were used as viscosifier and stabilizer and were obtained from Sigma Aldrich, USA. Polyanionic cellulose (PAC: molecular weight, 3.3 × 10^5 Da; degree of substitution of carboxylic group: 0.92) was supplied by Gumpro Drilling Fluids Pvt. Ltd (India), which was used as a fluid loss-controlling agent. Sodium lauryl sulphate (SLS) with an HLB index of 40 was used as an emulsifier to formulate oil-in-water emulsion-based mud. Diesel oil (color: yellow; density: 0.823 g·cm^{-3}; viscosity at 40 °C: 2.4 cSt) was obtained from a local fueling station and was used to prepare oil-in-water emulsion mud for comparison with the proposed MME mud.

2.2. Transesterification of mahua oil

Initially, the raw mahua oil was heated at 100 °C in a water bath for half an hour, and stirring was done to remove the unwanted water substance present in the raw oil. The heated oil was further filtered to eliminate undesired dirt and other pollutants. The transesterification process was carried out to convert the triglycerides in the oil into methyl esters (Knothe, 2005). A three-necked round-bottom flask (with a reflux condenser having a capacity of 500 mL) was taken, and 180 g of mahua oil was put into the flask. The bottom flask was set up on a magnetic stirrer with a temperature and speed controller. Meanwhile, 40 g of methanol (reactant) and 1.0 g of KOH (catalyst) were mixed before being added to mahua oil. The transesterification reaction was conducted at 200 rpm and 60 °C for 30 min. After completion, the solution mixture was placed into a separating funnel and left to settle for 12 h. After 12 h, the solution was separated into two distinct layers; the upper layer was crude MME, whereas the bottom layer was glycerol. The excess amount of methanol was removed through vacuum distillation, and the obtained MME was further purified by washing with 100 mL of warm water at 60 °C until its pH reached 7. After removing the water, the crude MME

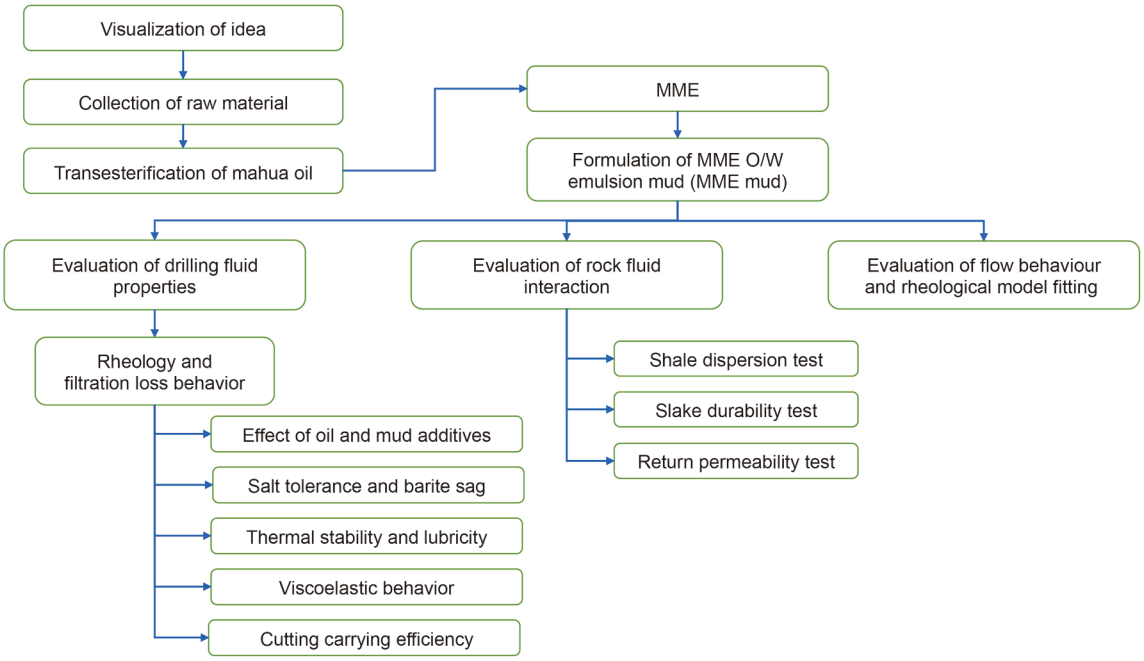

Fig. 1. The details of the research methodology employed in this study.

was heated on a hot plate at 100 °C with gentle stirring for 30 min to facilitate water evaporation. The remaining MME (pale yellow color) was collected and stored at room temperature. The typical physicochemical properties, such as density, kinematic viscosity, and acid value of synthesized MME, were determined using ASTM protocols. The details of the reaction scheme of the transesterification reaction of mahua oil are shown in Fig. 2.

2.3. Formulation of oil-in-water (O/W) mud

An O/W emulsion mud was formulated using MME. The MME was utilized as a dispersed phase, whereas deionized water was used as a continuous phase. Following the API recommended procedure (API RP 13B-2, 2019). The mud was prepared to get the mud weight of 10 ppg with an oil-water ratio of 20:80 for one laboratory barrel (equivalent to 350 mL). The composition of the base fluids of the O/W mud system is tabulated in Table 2. The additives were blended using an overhead laboratory stirrer (Model: Hamilton Beach Mixer) at a rotational speed of 8000 rpm. A dilution test was conducted to ascertain the formation of the desired oil-in-water emulsion by dropping the prepared formulation on the water surface. It was observed that the droplets dispersed in the water, confirming the formation of an oil-in-water emulsion.

2.4. Evaluation of drilling fluid properties

2.4.1. Rheology and filtration loss behavior

The rheology of formulated drilling fluid (Table 2) was measured using a viscometer (Make: Fann, Model: 35) as per recommended API protocols (API RP 13B-2, 2019). The prepared mud samples were put in a viscometer cup and sheared at 3, 6, 100, 200, 300, and 600 rpm, and the corresponding dial reading values were recorded. The experiments were conducted in triplicate, and average values were reported. The dial reading obtained from the viscometer is used to estimate rheological properties such as

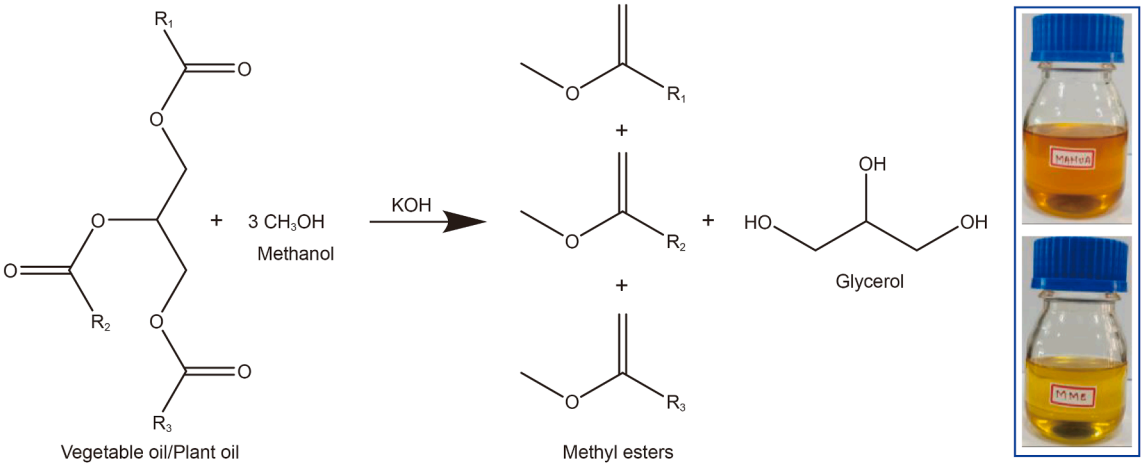

Fig. 2. Synthesis of mahua oil methyl ester using the transesterification reaction of mahua oil [inset: mahua oil and MME].

Table 2
Mud composition of O/W emulsion mud system.

Additives	Unit	Function	Order	MME mud	Diesel mud
Water	mL	Continuous phase	1	280	280
Clay	g	Viscosifier and fluid loss	2	7	7
XG	g	Primary viscosifier and emulsifier	3	1.75	1.75
PAC	g	Fluid loss control	4	1.4	1.4
CMC	g	Viscosifier and fluid loss	5	1.4	1.4
SLS	g	Emulsifier	6	2.1	2.1
Oil	mL	Dispersed phase	7	70	70
Barite	g	Weighing agent	8	68	68

apparent viscosity (AV), plastic viscosity (PV), and yield point (YP). The property AV is the ratio of observed fluid stress to the rate of shear and is typically measured at 600 rpm. PV refers to the resistance of the fluid to flow, which occurs in drilling mud due to mechanical friction between solids and liquids. YP represents the minimum shear stress necessary to initiate fluid flow. These properties are determined using Eqs. (1)–(3):

$$\mathrm{AV} = \frac{\theta_{600}}{2}\ (\mathrm{cP}) \tag{1}$$

$$\mathrm{PV} = \theta_{600} - \theta_{300}\ (\mathrm{cP}) \tag{2}$$

$$\mathrm{YP} = \theta_{300} - \mathrm{PV}\left(\mathrm{lb} \Big/ 100\ \mathrm{ft}^2\right) \tag{3}$$

where θ_{600} and θ_{300} represent the dial readings at 600 and 300 rpm, respectively. Gel strength (GS) is measured at a low shear rate after allowing the mud sample to remain undisturbed for 10 s and 10 min. To determine the gel strength, the cylinder is rotated at 3 rpm, and the maximum deflection is recorded before the gel structure breaks. Additionally, the consistency plots (shear stress *vs* shear rate) of the formulated MME mud samples were determined using an air-bearing rheometer (Make: Anton Par, Model: 102) equipped with a cup and bob geometry in dynamic mode to describe the flow behavior of the drilling mud system. The shear rate for the experiment was varied from 0.1 to 1000 s^{-1}. The obtained consistency plots were used to estimate rheological parameters of rheological models such as Bingham-Plastic (BP), Power Law (PL), Herschel-Bulkley (HB), Robertson-Stiff (RS), and Cross (CS). API filtration loss experiments were conducted at a pressure of 100 psi for 30 min to determine the filtration characteristics of the formulated mud samples (Table 2), and the filtration volumes were recorded at 1, 7.5, 15, 20, 25, and 30 min.

2.4.2. Thermal stability

To examine the effect of temperature on MME mud, a hot rolling aging test was performed at 120 and 150 °C under dynamic conditions of 30 rpm (API RP 13B-2, 2019). The rheological properties of each mud sample are measured both before and after hot rolling aging. Initially, the properties were measured under ambient conditions, referred to as before hot rolling (BHR). The mud samples were then placed in an aging cell inside a hot-roller oven (Make: Alliance Tech, Model: AT-HRO-2023) for 16 h. After the hot rolling process (AHR), the rheological properties were reassessed.

2.4.3. Viscoelasticity

The viscoelastic properties of formulated MME mud samples (Table 3) were evaluated using an air-bearing rheometer (Make: Anton Par, Model: 102) equipped with a cup and bob geometry. Before the start of the test, a pre-shear for 5 min at 1000 s^{-1} was applied to the sample, followed by a 10-min rest stage for the growth of the microstructure. The amount of deformation energy that is stored in the sample during a shear process is represented by the storage modulus (G'), and the amount of deformation energy that is used up and lost by the sample is represented by the loss modulus (G'') (Mezger, 2006). The linear viscoelastic range (LVER: the range of strains where the G' and G'' curves exhibit constant plateau values before the samples internal structure being shattered), dynamic yield point (YP_D), and flow point (FP) were estimated using amplitude sweep at 30 °C and a constant frequency of 6.25 rad/s with a strain amplitude ramp of 0.001%–1000%. Frequency sweep tests were conducted by varying frequencies from 100 to 0.001 rad/s at constant shear strain values of 0.05% and were used to investigate the time-dependent behavior and structural stability of formulated mud samples. Further, to assess gel recovery as a function of time, the time sweep test was performed with constant strain and frequency of 0.05% and 6.25 rad/s, respectively.

2.4.4. Salt tolerance

Salt tolerance is crucial to combat mud contamination problems that can arise from encountering salt during drilling operations. Drilling mud can become contaminated with salt from diverse geological formations, which degrades its effectiveness. MME emulsion muds were exposed to different salt concentrations (NaCl: 1.0–3.0 wt% and $CaCl_2$: 1.0–3.0 wt%) to evaluate their salt resistance and assess the impact on rheological and filtration properties.

2.4.5. Static sag test

A static sag test was conducted using a hot-roller oven to determine the suspension properties of MME emulsion muds. The MME mud samples were aged for 16 h at 120 °C. The mud samples used in the study were aged for 16 h at 120 °C under static conditions (rotation = 0 rpm). A syringe is used to collect a known volume of mud sample from the upper and lower parts of the cell to calculate its density. The measured densities of MME emulsion mud are used to calculate the sag factor using Eq. (4).

$$(\mathrm{Sag\ Factor})_{\mathrm{Static}} = \frac{\rho_{\mathrm{bottom}}}{\rho_{\mathrm{top}} + \rho_{\mathrm{bottom}}} \tag{4}$$

Table 3
Physicochemical properties of MME.

Properties	Mahua oil methyl ester
Color	Pale yellow
Appearance	Clear
Density, g·cm^{-3}	0.837
Kinematic viscosity at 40 °C, cSt	4.1
Acid value, mg KOH/g	0.5
Flash point, °C	129

2.4.6. Cutting carrying efficiency

Hole cleaning is a vital function of drilling fluid, ensuring the effective removal of cuttings from the wellbore to the surface. It is estimated using the dimensionless parameter known as the cuttings carrying index (CCI, Eq. (5)) as per the API recommended practice (API RP 13D, 2017):

$$\mathrm{CCI} = \frac{K \times V \times M_{\mathrm{w}}}{400000} \tag{5}$$

where K is the consistency index, V is the annular velocity feet per minute (ft/min), and M_{w} is the density of the prepared mud in pounds per gallon (ppg). The value of K was calculated using Eq. (6).

$$K = 511^{1-n} \times (\mathrm{PV} + \mathrm{YP}) \tag{6}$$

where n is the flow behavior index, PV is the plastic viscosity (cP), and YP is the yield point (lb/100 ft^2) obtained using dial readings (θ) at 600 and 300 rpm from the Fann VG meter. The flow behavior index (n) was calculated using Eq. (7).

$$n = 3.322 \log \frac{2 \times \mathrm{PV} + \mathrm{YP}}{\mathrm{PV} + \mathrm{YP}} \tag{7}$$

2.4.7. Lubricity

The lubricating behavior of the prepared MME mud sample was determined using a lubricity tester (Make: OFITE; Model: 112-00-1). The standard lubricity coefficient test was conducted at 60 rpm with 150 in-lb of force applied by a torque arm. Initially, a calibration for measuring the coefficient of friction (CoF) was performed using deionized water, and a correction factor corresponding to deionized water was obtained using relation (Eq. (8)).

$$\text{Correction factor (CF)} = \frac{34(\text{Standard reading made for deionized water})}{\text{Observed water reading}} \tag{8}$$

Finally, the test cup was filled with the test sample, and the test was conducted for 5 min. The final torque reading was recorded, and CoF was determined using Eq. (9).

$$\mathrm{CoF} = \frac{\text{Meter reading} \times \text{Correction factor}}{100} \tag{9}$$

2.5. Emulsion stability using zeta potential

The zeta potential of the MME mud system was measured using the laser Doppler electrophoresis method (Make: Anton Paar, Model: Lite-sizer 500). The prepared mud test samples were diluted in deionized water in a ratio of 1:50. The solution was poured into a disposable cuvette, and the zeta potential value was measured. All the measurements were conducted in triplicate at a temperature of 25 °C by selecting the Huckel approximation. Additionally, the effect of thermal aging on the colloidal stability of the formulated mud system was evaluated by measuring the zeta potential of the mud samples after subjecting them to hot rolling at 120 °C (AHR).

2.6. Evaluation of rock-fluid interaction

2.6.1. Shale dispersion test

The shale dispersion test was performed to ascertain the effectiveness of prepared MME emulsion mud samples in maintaining the integrity of the cuttings and to determine the interaction of cuttings with prepared mud samples. The shale dispersion test was conducted as per the API standard testing protocol (API RP 13I, 2023). The shale used in this study was obtained from the Damodar Valley Basin, India. X-ray diffraction analysis (Make: Panalytical, Model: Empyrean-QTY1) was done to identify and determine the bulk mineralogical composition. Based on the characteristic 2θ values, the shale was found to be composed of quartz (35.96%), muscovite (34.33%), kaolinite (15.54%), and siderite (14.17%). The details of the XRD analysis are provided in Supplementary Information (Fig. S1).

For the shale dispersion test, 150 g (W_{o}) of screened shale fragments (passing through mesh 10 and retaining at mesh 16) along with 350 mL of drilling fluid were placed in an aging cell and subjected to dynamic aging in a hot roller oven at a temperature of 120 °C for 16 h. After 16 h, the aging cell was cooled at ambient temperature, and mud was poured over a sieve. The retained shale sample pieces are retrieved, cleaned, weighed, and dried overnight at 60 °C in an oven. Then, the shale sample weight was measured (W_1) to calculate the shale recovery (R_1) in percent. Additionally, to establish a baseline for the assessment of shale reactivity, the primary recovery (R_1) was performed using deionized water to simulate clay-freshwater interaction in near-well or swept zones, which is essential to determining the maximum possible dispersion tendency of the shale. Further, to assess the longevity of the effect of the formulated MME emulsion mud in inhibiting the dispersion of cutting, a re-run dispersion test was performed. In this test, the above-obtained dried sample was added to the aging cell containing 350 mL of deionized water and heated at 120 °C for 16 h in the roller oven. After 16 h of aging, the sample was cooled, collected, and dried overnight at 60 °C in an oven. Finally, the weight of the shale sample (W_2) was recorded to calculate the second shale recovery (R_2) in percent. The following equations (Eqs. (10) and (11)) were used to compute the shale recovery on a dry mass basis (Khodja et al., 2010).

$$R_1 = \frac{W_1}{W_{\mathrm{o}}} \times 100\% \tag{10}$$

$$R_2 = \frac{W_2}{W_{\mathrm{o}}} \times 100\% \tag{11}$$

2.6.2. Slake durability index

The slake durability test was performed to determine the resistance of shale samples (treated as cuttings) to weakening and disintegration arising from a regular drying and wetting cycle. A standard testing procedure suggested by Franklin and Chandra (1972) was followed to estimate the slake durability index. Prior to the test, the sieved shale cuttings were dried at 120 °C in an oven for 16 h. A 350 g of dried shale cutting (W_{I}) was placed in a wire mesh drum of 2 mm mesh size. The mesh drum was rotated at 20 rpm for 10 min while being partially submerged in the formulated MME mud system kept inside the trough. In addition, the drum was taken out of the trough and dried in the 120 °C oven. After that, the total weight (W_{F}) of the drum and the preserved shale sample was recorded. Afterward, the drum was thoroughly

cleaned, and its weight (W_D) was noted. The slake durability index (I_d) is defined as the final to initial weight percent of the dry shale sample and is determined using Eq. (12).

$$I_d = \frac{W_F - W_D}{W_I - W_D} \times 100\% \quad (12)$$

2.6.3. Return permeability test

The return permeability test (RPT) aims to determine the reduction of permeability induced by the invasion of drilling mud into oil and gas reservoirs during the drilling process. The RPT was conducted by adopting the methodology described by Yonebayashi et al. (2017). The test was performed using a core flooding setup (Make: DCAM) comprising two fluid collectors, a syringe pump, a core holder, and a measuring cylinder to measure the effluent volume. For this test, a core of length 4.8 cm, diameter of 2.2 cm, and porosity of 0.41 was considered, and all experiments were performed at a controlled temperature of 30 °C. The core was initially flooded using KCl brine (23.47 wt%) to measure initial permeability (K_i), and then the drilling fluid was injected into the core to simulate downhole drilling conditions. After the injection, the core was reversed and further flushed with KCl brine to measure the final permeability (K_f). The return permeability (R_f) is calculated using $R_f = \left(\frac{K_f}{K_i}\right) \times 100\%$. To ensure reproducibility, the core flooding experiments were performed in triplicate on the clean core extracted from the same sandstone block. The average differential pressure values were used to calculate the initial and final permeability. The core used in this study was drilled from the block sandstone rock sample obtained from Jodhpur, India. X-ray diffraction analysis was done to identify and determine the bulk mineralogical composition of the sample. Based on the characteristic 2θ values, the sandstone core sample was found to be composed of quartz (61.58%), kaolinite (19.18%), muscovite (12.40%), and orthoclase (6.84%). The details of the XRD analysis are provided in Supplementary Information (Fig. S2).

3. Results and discussion

3.1. Transesterification of mahua oil

The transesterification of mahua oil was confirmed using FTIR analysis. Fig. 3 shows the FT-IR plots of raw mahua oil and synthesized mahua oil methyl ester (MME. The characteristic peak of triglyceride in raw mahua oil appears at 1746 and 1153 cm^{-1}, due to the stretching and bending vibration of the carbonyl (O–C=O) group, respectively, within the triglyceride molecule of a complex glycerol backbone. However, in MME, the stretching vibration of the carbonyl (O–C=O) group was observed at a slightly lower wavenumber, i.e., 1739 cm^{-1} (Kania et al., 2021), whereas the bending vibration was observed at a slightly higher wavenumber, i.e., 1170 cm^{-1}. The shift in wavenumber is attributed to the change in the chemical environment of the carbonyl group arising due to the replacement of the complex ester linkage in triglycerides of mahua oil with the simpler methyl ester group in MME. The electron-donating methoxy ($-OCH_3$) group in MME increases electron density around the carbonyl functional group (O–C=O) and, thus, slightly strengthens the O–C bond and weakens the C=O bond. This results in a higher bond force of the O–C bond and a lower bond force of the C=O bond, thus resulting in the shifting of the corresponding peaks to higher and lower wavenumber, respectively (Socrates, 2004). Further, the peak corresponding to the methyl group ($-CH_3$) of methyl ester was observed at

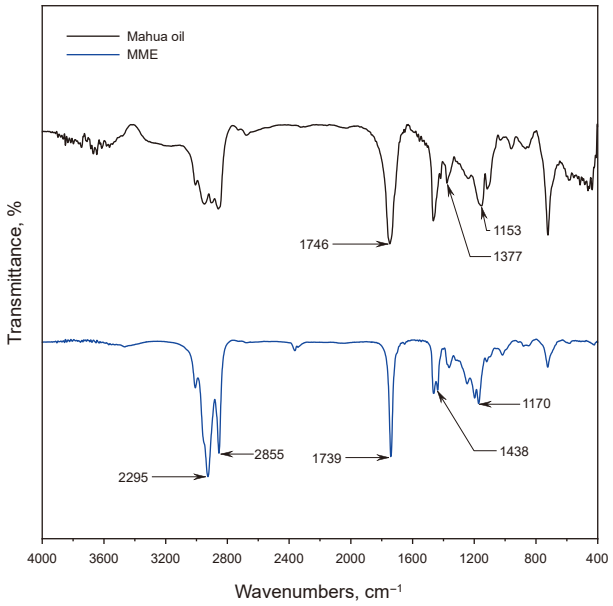

Fig. 3. FT-IR spectra of mahua oil and MME.

1438 cm^{-1} and was found to be absent in the mahua oil sample. The peak at 1377 cm^{-1} in raw mahua oil, attributed to the glycerol group (O–CH_2), was absent in the spectrum of MME (Rabelo et al., 2015). Additionally, no peaks were observed in the wavenumber range of 3200 through 3570, indicating the absence of residual fatty acid, unreacted methanol, or water in the MME samples. The combined presence of the ester-specific bands, appearance of the $-CH_3$ peak, the absence of the glycerol group, and the shifting of the stretching and bending vibration of the carbonyl group confirm the formation of long-chain fatty acid methyl esters (FAMEs). The physicochemical properties of MME are presented in Table 3. The percentage yield of methyl ester $\left(\text{Yield} = \frac{\text{Methyl ester obtained}}{\text{Weight of raw oil}} \times 100\%\right)$ was estimated to be 89.1% (Sabariswaran et al., 2014).

3.2. Evaluation of drilling fluid properties

3.2.1. Rheology and filtration loss behavior

The rheology of the drilling fluid is one of the crucial properties that govern flow features, cutting carrying efficiency, and hydraulics during drilling operations (Caenn and Chillingar, 1996). Further, the rheological characteristics (AV, PV, YP, and GS) of mud significantly impact drilling parameters such as hole clean-up, borehole hydraulics, mud cake structure, rate of penetration, and stability. The dependence of rheology on several aspects of drilling and well stability makes it a crucial property and requires a proper understanding both before and during drilling operations. Another crucial aspect of drilling is the filtration volume, which must be kept to a minimum to prevent formation damage and wellbore instability (Tiwari et al., 2020).

3.2.1.1. Effect of oil on mud. The rheological and filtration properties of prepared mud samples (Table 2) were determined using a Fann VG meter and API filter press, respectively. The details of observed dial reading at 3, 6, 100, 200, 300, and 600 rpm are shown in Fig. 4(a). The dial reading values were used to calculate rheological parameters such as AV, PV, and YP. The details of estimated rheological parameters (AV, PV, and YP), gel strengths,

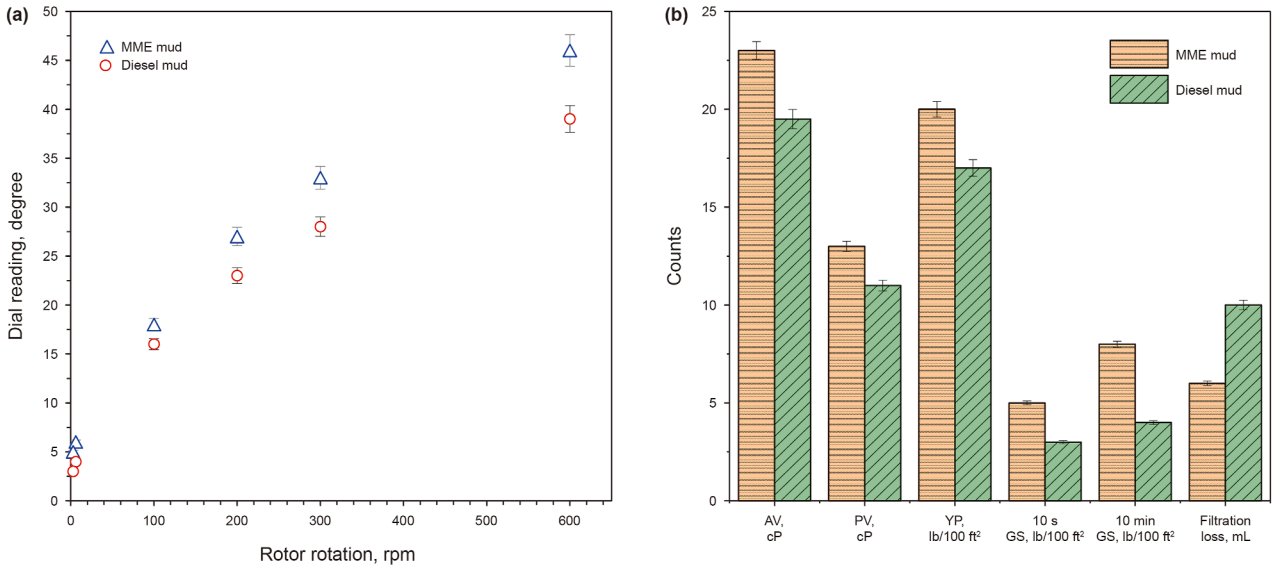

Fig. 4. (**a**) Fann viscometer readings for MME and diesel oil-based emulsion mud; (**b**) Estimated rheological (AV, PV, YP, 10 sec- and 10 min-gel strength) and filtration loss properties.

and fluid loss volume are shown in Fig. 4(b). According to the laboratory investigation, the MME mud shows significantly higher values of AV, PV, and YP than diesel oil-based mud. Despite both having identical additive content, the AV, YP, and PV of the MME mud were greater than those of the diesel mud by 17.9%, 17.6%, and 18.1%, respectively. The enhanced viscosity (AV and PV) of MME mud is attributed to the higher kinematic viscosity of MME (4.1 cSt) as compared to diesel oil (2.6 cSt), resulting from the presence of a long-chain oxygen-containing ester functional group, which increases intermolecular interaction (Bai et al., 2021). Additionally, the oxygen-containing ester group gets adsorbed to the clay surface via polar attraction, promoting a flocculated network structure that results in higher YP values. The YP/PV ratio, a measure of cutting lifting capacity and structural stability of drilling mud, was estimated using the measured YP and PV values. A higher YP/PV ratio indicates a dominant gel structure of drilling fluid with good cutting transport and hole-cleaning ability. In contrast, a lower YP/PV ratio indicates a lower tendency for gas cutting, lower swabbing, and higher structural stability of mud (Chilingarian et al., 1986). However, if not in range, the higher YP/PV ratio leads to coagulation and flocculation of mud, whereas the lower YP/PV ratio leads to inadequate hole cleaning (Kania et al., 2021). Therefore, the YP/PV ratio should be in the optimal range to maximize cutting transport efficiency while minimizing mud coagulation and flocculation. The prescribed desirable range of the YP/PV ratio is mentioned to be 1.0–2.0 (Gautam and Guria, 2020). It is observed that despite different rheological behaviors, the YP/PV ratio of both MME and diesel-based mud systems was found to be identical, i.e., 1.54, indicating similar cutting lifting capacity and structural stability of both the muds. Hence, MME is a suitable alternative to diesel for the formulation of O/W emulsion-based mud. Additionally, the gel strength (Fig. 4(b)) of MME emulsion mud was found to be higher than that of diesel oil emulsion-based mud. However, both initial gel strength and final gel strength remain in the desired range of 6–10 and 8–12 lb/100 ft^2, respectively (Sulaimon et al., 2017). Therefore, the MME mud is suitable for preventing cuttings and weighing materials from settling during static conditions. Additionally, the desirable gel strength of mud makes it ideal for utilization in drilling a deviated or horizontal well with a prominent gravity effect. The mud may prevent the accumulation of solids on the lower side of the borehole, thus preventing blockage (Caenn et al., 2011). The filtration loss volume of MME mud was found to be lower than that of diesel mud, indicating a superior filtration control characteristic. The superior filtration behavior of the MME mud is attributed to the polar interaction of oxygen oxygen-containing ester functional group with the clay particles, which leads to the formation of a networked structure (Ahmed et al., 2021). Additionally, the higher viscosity of MME mud provides higher resistance to filtrate flow. Thus, leading to further improvement in filtration control performance (Tiwari et al., 2020).

3.2.1.2. Effect of polymers. The MME mud (Table 2) comprises xanthan gum (XG), polyanionic cellulose (PAC), and carboxymethyl cellulose (CMC); the effect of individual polymers on rheological and filtration control characteristics was studied by varying the loading of individual polymers. The details of the impact of individual polymers, i.e., XG, PAC, and CMC, on rheological properties such as AV, PV, YP, and 10 s and 10 min GS are shown in Fig. 5(a–c), and the effect of individual polymers on fluid loss volume is shown in Fig. 5(d).

The effect of XG biopolymer on the rheological properties of formulated MME mud was analyzed with increased loading from 0.3 to 0.7 wt%. From Fig. 5(a), the value of AV, PV, YP, and GS of MME mud formulation was observed to increase with an increase in XG loading. The increase in plastic viscosity (PV: from 10 to 20 cP) is attributed to the viscosifying nature of the XG biopolymer, which forms a complex network structure through the adsorption of its polar groups (carboxyl and hydroxyl) onto bentonite particles (Wei et al., 2022). The formation of a complex network structure also leads to resistance of the flow under low shear rates, which leads to a significant increase in the YP values (i.e., from 18 to 28 lb/ft^2). The entanglement of long-chain XG polymer at a high shear rate causes an increase in AV values, i.e., from 19 to 34 cP. The increase in both YP and PV values leads to a slight decrease in the YP/PV ratio; however, the ratio remains in the desired range between 1 and 2.

Similarly, the effect of polyanionic cellulose (PAC) was established by varying the loading of PAC from 0.3 to 0.7 wt% in MME

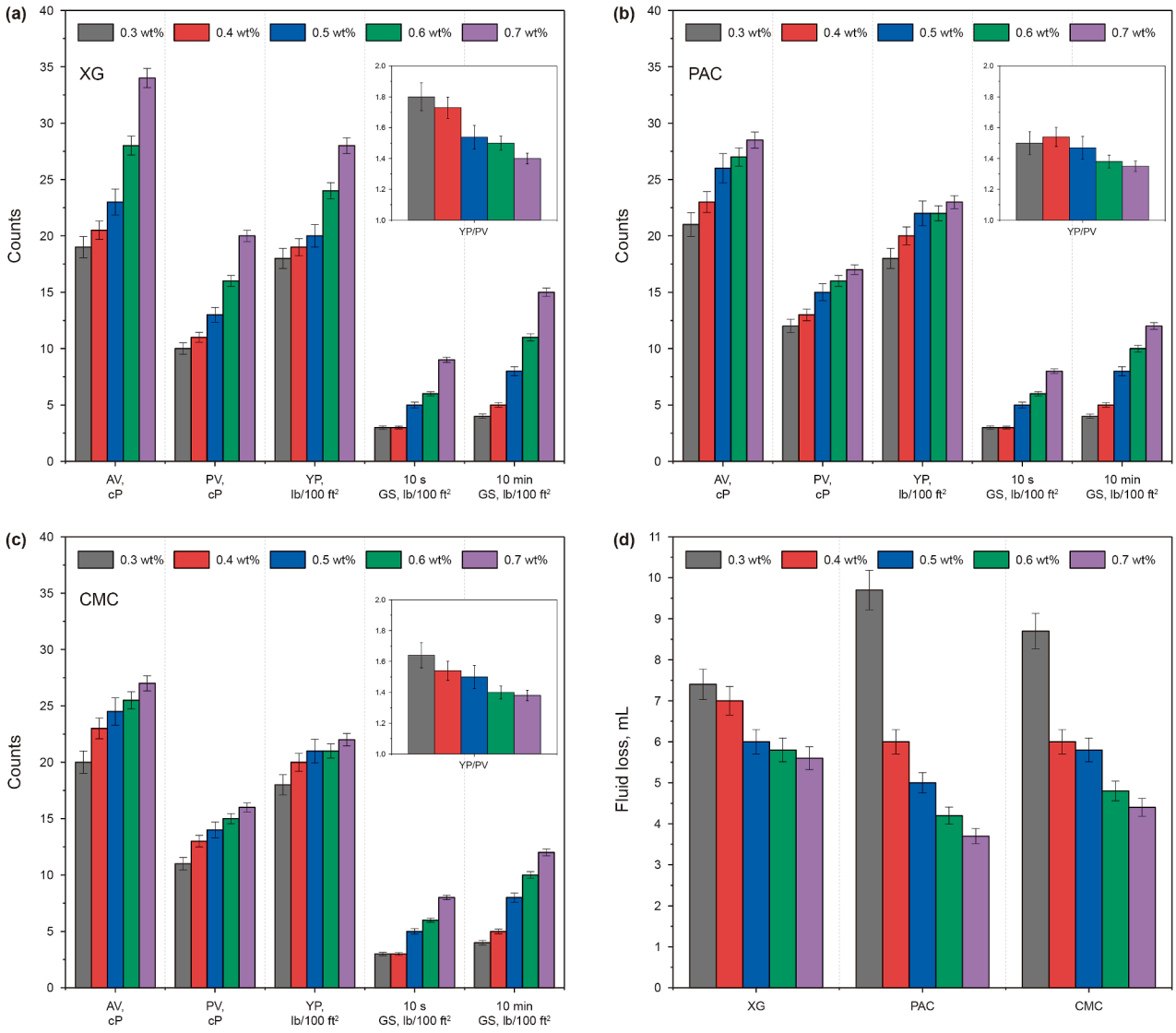

Fig. 5. Effect of polymer loading (**a**) XG, (**b**) PAC, and (**c**) CMC on rheological parameters (AV, PV, and YP, and 10 s and 10 min gel strength), and (**d**) effect of individual polymer on fluid loss volume.

mud formulation. The details of AV, PV, YP, 10 s- and 10 min-gel strength with varying PAC are shown in Fig. 5(b). Interestingly, an increase in rheological properties (AV, PV, YP, and GS) was observed with an increase in PAC concentration, attributed primarily to the creation of the network and binding with bentonite platelets (Li et al., 2024). However, the increase in viscosity is less prominent than that observed with XG as the molecular weight of PAC (3.3×10^5 Da) is less than that of XG (1.1×10^6 Da), and therefore, PAC behaves as a filtration control additive with less effect on rheology than XG biopolymer. Fig. 5(c) shows the effect of CMC loading on rheological properties. Like the PAC biopolymer, the rheological parameters (AV, PV, and YP) of MME mud increased with CMC loading. The increase in viscosity is due to the presence of the sodium carboxymethyl group in the CMC, which releases the Na^+ ion in an aqueous solution, making it anionic and hydrated. Over the hydration period, the adsorbed molecules provide the polymer with an extended structure, increasing the viscosity of MME mud. The increase in viscosities (AV and PV) was less prominent than that observed with PAC, which has a similar molecular structure to CMC. However, the PAC has a higher degree of substitution than CMC (PAC: 0.92 > CMC: 0.51), i.e., more hydroxyl groups (−OH) on the cellulose backbone are replaced with anionic carboxymethyl group (−CH_2−COOH). It is interesting to note that, with the highest loading of XG, PAC, and CMC, the YP/PV ratio of the mud system remained in the desired range, i.e., between 1 and 2, indicating excellent compatibility with the MME mud system with the traditional biopolymers and showed no visible sign of coagulation or flocculation. Thus, the MME may be used as a replacement for diesel in the formulation of oil-based mud.

The filtration properties of MME mud were analyzed by varying the loading of individual polymers (XG, PAC, and CMC) from 0.3 to 0.7 wt%. The effect of individual polymers on filtration loss volume is shown in Fig. 5(d). It was observed that fluid loss volume decreased with increased loading of all polymers. However, the decrease was more prominent in PAC, i.e., from 10 to 3.7 mL. The superior filtration control by PAC is chiefly attributed to the absorption of negatively charged carboxylic groups of PAC onto the positively charged edge of clay platelets via the formation of electrostatic attraction (Li et al., 2016a), resulting in the formation of a networked microstructure. It is mentioned that API

recommends a filtration loss volume of less than 10 mL/30 min for adequate filtration control (Arain et al., 2022), thus making the MME mud a suitable choice for drilling.

3.2.1.3. Effect of clay. To study the effect of clay on the rheological and filtration properties of MME mud, the concentration of clay varied from 1.5 to 3.5 wt%. The details of rheological behavior (AV, PV, YP, 10 s- and 10 min-gel strength) and filtration behavior with varying loading of clay content are shown in Fig. 6(a) and (b), respectively.

It is observed that with an increase in the loading of clay from 1.5 to 3.5 wt%, the AV and PV values of the mud sample increased from 20 to 39 cP and 12 to 21 cP, respectively. The increase in viscosity (AV and PV) and yield point (YP) is attributed to the enhanced interaction among clay particles by virtue of attractive (van der Waals forces) and repulsive (electrostatic) forces, forming a networked structure that resists shear, thus contributing to higher viscosity (William et al., 2014). The YP/PV ratio of the mud samples was found to increase with the increase in the clay content. However, the ratio remained in the desirable range of 1–2. This behavior may be attributed to increased particle-particle interactions, making the drilling fluid more susceptible to coagulation or flocculation (ASME, 2005). The increase in the YP/PV ratio is an early sign of the decrease in fluid stability, which may further deteriorate in the presence of salt contamination (Chilingarian et al., 1986). Additionally, the fluid loss volume was found to decrease with an increase in clay concentration. However, the thickness of the observed mud cake was found to increase with the clay concentration due to an increase in clay content. The reduction in fluid loss volume is due to the formation of a denser and more compact filter cake, which reduces the permeability of the cake, resulting in reduced filtration volume (Abed and Rasaei, 2024). Additionally, the swelling of clay particles results in high gel strength and consequently leads to the sealing of the pores of the filter paper, thus reducing the volume of fluid loss.

3.2.2. Thermal stability of drilling fluid

The effect of temperature on MME and diesel mud was evaluated by subjecting the mud samples to a hot rolling aging test in a roller oven for 16 h. The details of drilling fluid properties before (BHR) and after hot rolling (AHR) aging test are presented in Table 4. It is observed that the rheological properties (AV, PV, YP, and GS) of MME mud marginally decreased with an increase in aging temperature, indicating the thermal stability of the mud and the absence of temperature-induced gelation. The enhanced thermal stability of the MME mud is attributed to the presence of the methyl ester functional group ($-COOCH_3$), which contributes to strong dipole-dipole interaction, requiring higher thermal energy to overcome thermal decomposition and structural breakdown (Atkins et al., 2023). In contrast, the diesel mud initially showed a slight decrease in viscosity at an aging temperature of 120 °C. However, on further increase in temperature, i.e., at 150 °C, a sharp decrease in viscosity (AV and PV) and gel strength was observed. This behavior is attributed to the decomposition of diesel oil at temperatures above 120 °C, resulting in destabilization of the O/W emulsion and destruction of the networked gel

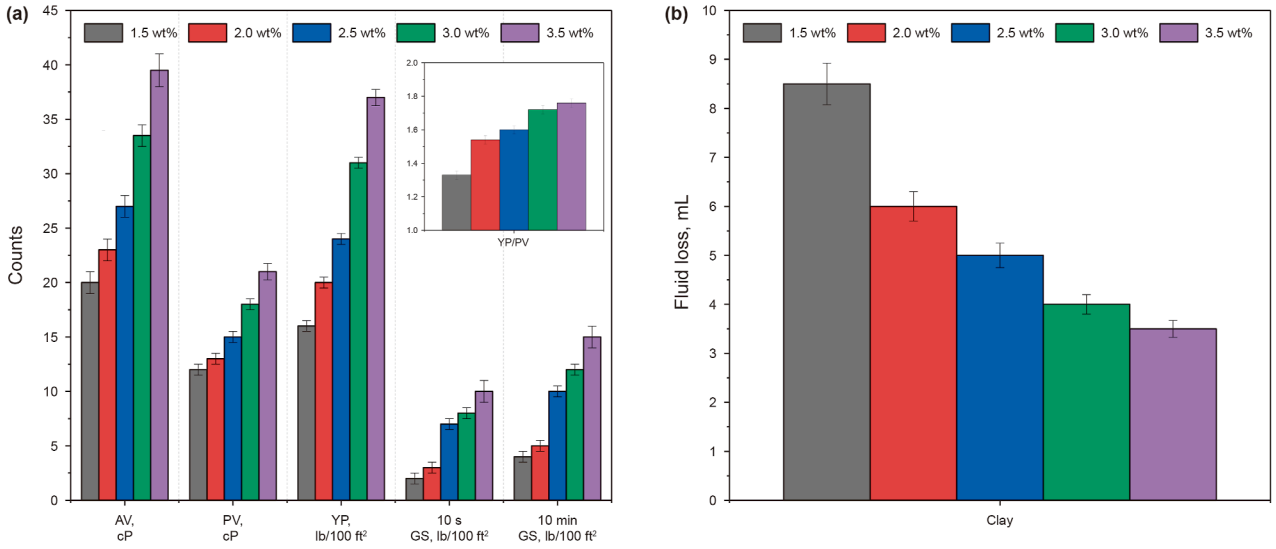

Fig. 6. Effect of clay concentration on (**a**) rheological properties and (**b**) filtration loss of MME mud.

Table 4
The effect of the hot rolling aging test on rheology, lubricity, and filtration behavior of MME and diesel O/W emulsion mud.

	MME mud			Diesel mud		
	BHR	AHR		BHR	AHR	
	(Ambient)	120 °C	150 °C	(Ambient)	120 °C	150 °C
AV, cP	23.0	21.0	19.5	19.5	17	10.5
PV, cP	13.0	11.0	10.0	11	10	11
YP, lb/100 ft^2	20.0	20.0	19.0	17	14	5.0
YP/PV	1.54	1.82	1.90	1.55	1.40	2.20
Initial gel strength, lb/100 ft^2	5.0	4.0	3.0	3	2.5	1.5
Final gel strength, lb/100 ft^2	8.0	7.0	5.0	4	3	2.5
API filtration loss, mL	6.0	6.3	6.9	10.0	12.1	17.4

structure of drilling mud. Additionally, API filtration loss (FL) of mud samples was also observed to increase with aging temperature. However, the FL of MME mud remained within the acceptable limit (FL < 10 mL) at 150 °C. In contrast, the FL of diesel mud was 17.4 mL at 150 °C, further confirming the degradation and destabilization of diesel mud.

3.2.3. Flow behavior and rheological modelling

The flow behavior of the formulated MME mud was determined using an air-bearing rheometer in a shear rate range of 0.1–1000 s^{-1}. The details of the obtained shear stress (τ) vs. shear rate ($\dot{\gamma}$) plot and corresponding viscosity (η) vs. shear rate ($\dot{\gamma}$) plot are shown in Fig. 7(a). The shear viscosity of the mud sample was found to decrease with an increase in shear rate, showing a typical non-Newtonian shear thinning behavior. To further describe the non-Newtonian rheological behavior of the MME mud, mathematical modeling was performed to identify the best-fitted rheological models. In this study, commonly used rheological models, such as BP, PL, HB, RS, and CS models, were considered for characterizing the rheology of MME mud. These rheological models are used to establish the relationship between the measured shear stress (τ) and shear rate ($\dot{\gamma}$) values. The BP and PL models were fitted using linear regression, whereas the generalized reduced gradient search algorithm was adopted to estimate the model parameters of HB, RS, and CS models. The objective function of the algorithm was set to minimize the sum of squares of residuals $\left[\text{SSR} = \sum_{i=1}^{n}\left(\tau_{\text{actual},i} - \tau_{\text{model predicted},i}\right)^2\right]$. Additionally, coefficient of determination(r-squared) i.e., $R^2\left(=1-\frac{\text{SSR}}{\text{TSS}}\right)$ was determined to quantify the goodness of fit of the above rheological models (TSS, total sum of squares $= \sum_{i=1}^{n}(\tau_1 - \overline{\tau})^2$). It is mentioned that the R^2 values vary from 0 to 1, where 1 indicates a perfect fit of the model to the experimental data. The details of rheological models, initial guesses, model constraints, and fitting statistics (SSR and R^2) are presented in Table 5. The comparison of experimental and model-fitted shear stress values for BP, PL, HB, RS, and CS models is shown in Fig. 7(b).

Based on the rheological modeling, the SSR was found to follow the order BP > PL > CS > RS > HB, with the HB model having the lowest SSR value of 5.57. Fig. 7(b) reveals that the HB model provides a better fit for the overall shear rate range. Thus, the three-parameter HB model was found to be the most accurate model for describing the rheology of the MME mud. It is mentioned that

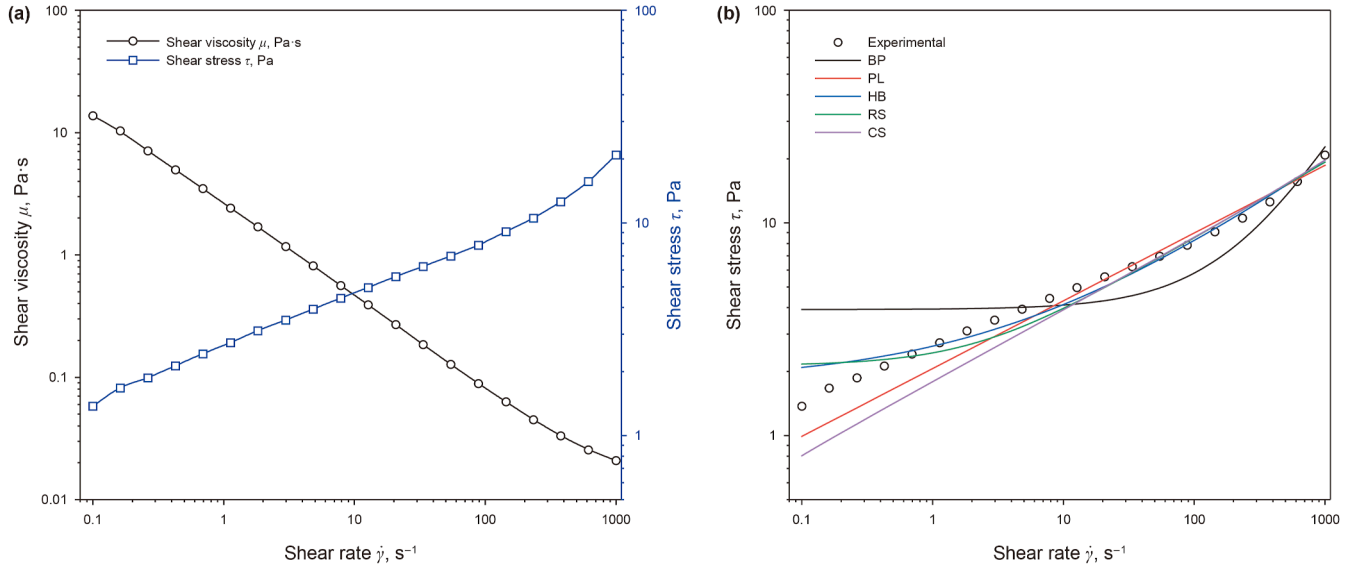

Fig. 7. (**a**) Shear stress vs. shear rate and corresponding shear viscosity plots of MME mud, and (**b**) comparison of the experimental and model fitted shear stress values for BP, PL, HB, RS, and CS model.

Table 5
The details of rheological models, corresponding initial guess, and constraints used for model fitting of rheology data, and corresponding estimated parameters and fitting statistics (SSE and R^2 values).

Model	Model equation	Initial guess and constraints	Parameters	Fitting stats
BP	$\tau = \tau_o + \mu_p\dot{\gamma}$	IG: $\tau_o = 0$ and $\mu_p = 0.05$ Constraints: $\tau_o \geq 0$ and $\mu_p > 0.05$	τ_o: 3.914 Pa μ_p : 0.019 Pa·s	SSR: 54.7 R^2: 0.8919
PL	$\tau = k\dot{\gamma}^m$	IG: $k = 1$ and $m = 0.5$ Constraints: $k > 0$ and $0 < m < 1$	k: 2.063 (Pa·s)^n m: 0.318	SSR: 12.39 R^2: 0.9777
HB	$\tau = \tau_o + k\dot{\gamma}^m$	IG: $\tau_o = 0$, $k = 1$ and $n = 0.5$ Constraints: $\tau_o \geq 0$, $k \geq 0$ and $0 < m < 1$	τ_o: 1.782 Pa, k: 0.8489 (Pa·s)^n n: 0.4414	SSR: 5.57 R^2: 0.9890
RS	$\tau = A(\dot{\gamma} + C)^B$	IG: $A = 1$, $B = 0.5$ and $C = 0$ Constraints: $A > 0$, $0 < B < 1$ and $C \geq 0$	A: 1.617 B: 0.3587 C: 2.1668	SSR: 8.951 R^2: 0.9825
CS	$\tau = \dot{\gamma}\left[\mu_\infty + \frac{\mu_o - \mu_\infty}{1 + (\alpha\dot{\gamma})^{\frac{2}{3}}}\right]$	IG: $\mu_o = 0.1$, $\mu_\infty = 0.05$ and $\alpha = 1$ Constraints: $\mu_o \geq 0$, $\mu_\infty \geq 0$ and $\alpha \geq 1$	μ_o: 193.16 Pa·s μ_∞: 0.0017 Pa·s α: 1105	SSR: 12.15 R^2: 0.9873

τ_o: yield stress; μ_p: plastic viscosity; k: consistency index; m: flow behavior index; A, B and C: RS model parameter; μ_o: zero-shear viscosity, μ_∞: infinite shear viscosity, and α: cross model constant.

the precise estimation of rheological parameters leads to the exact calculation of mud hydraulics, ensuring optimal wellbore cleaning, precise pressure loss prediction, efficient pump performance, and proper control of equivalent circulating density, thereby enhancing overall drilling efficiency and wellbore stability (Gautam and Guria, 2022).

3.2.4. Evaluation of viscoelastic properties

3.2.4.1. Amplitude sweep. Dynamic oscillatory measurement using an air-bearing rheometer was used to examine the viscoelastic properties of MME mud (Table 2). The variation of storage modulus (G'), loss modulus(G''), and shear stress (τ), obtained from the oscillatory amplitude sweep test of MME mud, is shown in Fig. 8. The linear viscoelastic range (LVER), a sign of a stable gel structure, is characterized by constant values of G' and G'' and represents the maximum strain the sample can withstand before the internal structure is destroyed. The LVER of the mud sample was determined to be 0.136%. It is also observed that the G' consistently remained higher than the G'' in the LVER, indicating the predominance of a solid gel-like structure in MME mud. Additionally, the greater G' over G'' values confirm that the MME-based drilling fluid is entirely composed of pure dispersion and emulsion (Werner et al., 2017). The gel-like behavior of MME mud persisted up to the crossover point, where G' equals G''. At this point, the oscillatory strain exceeds the threshold of the particles and droplets, causing them to leapfrog. This results in a complete breakdown of the structure and a subsequent decrease in G' values (Werner et al., 2017). Additionally, the YP_D and FP were estimated based on the τ data obtained from the oscillatory amplitude sweep test. The YP_D corresponds to the end of the constant G' plateau region (i.e., the shear stress corresponding to the end of LVER) and represents the stress at which the material begins to deform plastically or exhibits non-linear behavior. In contrast, the FP corresponds to the stress at the crossover point between the G' and G'' and marks the transition of the material from a stable gel-like state to a fully flowing state (Chen et al., 2023). The region between YP_D and FP is termed the yield zone. From Fig. 8, the YP_D of MME mud was found to be 0.92 Pa, while the FP was found to be 3.65 Pa. It is interesting to note that API recommends the measurement of low-shear yield point, a parameter similar to dynamic yield point, such that $LSYP = 0.51 \times (2\theta_3 - \theta_6)$ Pa. The LSYP is used to assess the ability of drilling fluid to suspend solids under very low shear conditions.

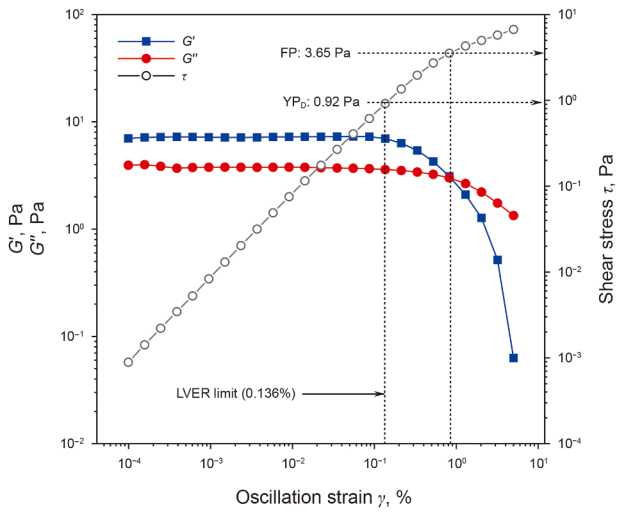

Fig. 8. Variation of storage (G'), loss (G'') modulus, and shear stress (τ) with oscillation strain for MME mud sample.

Additionally, it provides insight into the structural integrity of drilling fluid when at rest or under minimal agitation (Power and Zamora, 2003). Based on the Fann VG meter readings (Fig. 4(a)), the LSYP of the formulated MME mud sample was estimated to be 2.04 Pa, which lies in the yield zone region (i.e., YP_D < LSYP < FP). The above observations confirm the accuracy of the rheological data obtained using the Fann VG meter against the highly sophisticated air-bearing rheometer.

3.2.4.2. Frequency and time sweep. Fig. 9(a) shows the variation of G' and G'' for MME mud samples as a function of frequency (time). It is observed that the values of G' are always greater than G'' throughout the entire test frequency range. Thus, the test sample behaves like a viscoelastic solid, and its response to deformation is elastic under both fast and slow deformation conditions. This consistently higher G' value over G'' across the entire test frequency range indicates that the mud maintains a strong internal structure over time and is entirely made up of a stable gel, which is essential for suspending drill cuttings during periods of low or no flow. This gel-like, elastic-dominant behavior suggests that the mud can resist structural breakdown under both prolonged static conditions and repeated mechanical stress, such as during circulation-start-stop cycles. Additionally, it prevents the settling of weighting agents, thereby maintaining uniform density and rheological properties. Furthermore, the dominant elastic behavior of the mud system minimizes fluid loss into porous formations, thereby improving the filtration performance of the drilling fluid (Bui et al., 2012).

A time sweep test (Fig. 9(b)) was conducted to assess the evolution of the structure of MME mud over an extended period. For emulsion-based mud, the gelling time of the sample refers to the period during which the sample attains a stable gel structure, typically characterized by the plateauing of the storage modulus (G') (Werner et al., 2017). In the present study, stabilization of both storage and loss moduli was observed after 400 s, confirming the formation of a stable gel network that is essential for improving the suspension capacity of the mud under static and low-shear conditions.

3.2.5. Salt tolerance and barite sag

The influence of salt contamination (NaCl and $CaCl_2$) on the rheological properties and fluid loss behavior of MME mud was analyzed by adjusting the salt concentration within the range of 0.0–3.0 wt%. The specific effects of NaCl and $CaCl_2$ on these properties are presented in Table 6.

The results in Table 6 indicate a decrease in rheological properties (AV, PV, YP, and GS), while FL volume was found to increase with the increase in salt contamination. The reduction in the observed rheological values is primarily attributed to the salt screening effect (Sönmez et al., 2013). It is mentioned that a typical drilling fluid comprising polymeric additives achieves viscosity by virtue of the hydration thickening effect, whereas filtration loss characteristics are achieved by the absorption of polymer on bentonite (clay) platelets, leading to the formation of an impervious networked layer which aids in fluid loss control (Gautam et al., 2025). However, when exposed to monovalent cations of NaCl and divalent cations of $CaCl_2$, the negatively charged functional groups of polymers (XG, PAC, and CMC) become shielded by the salt (Guo et al., 2015). This shielding effect weakens the repulsive forces between these negatively charged groups, causing a reduction in viscosity and the ability to form a network, which in turn leads to inadequate fluid loss control. Additionally, it is observed that calcium contamination has a more adverse effect on rheology and filtration performance than sodium salt, resulting from the higher ion shielding effect of divalent calcium salt

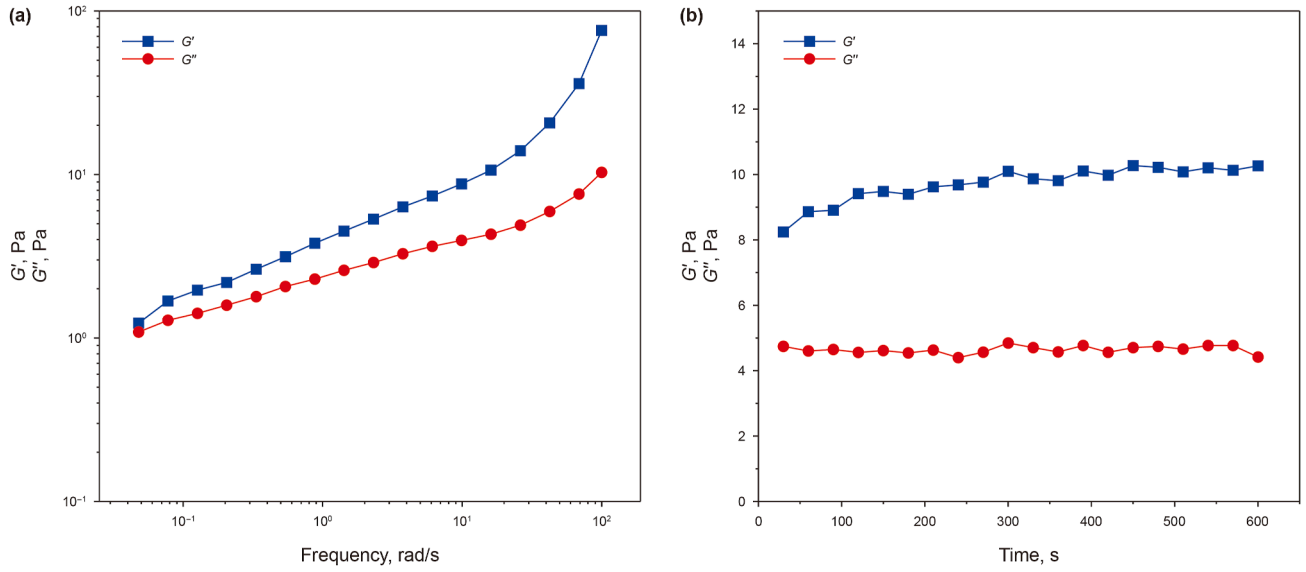

Fig. 9. (**a**) Variation of storage (G') and loss (G'') modulus with oscillation frequency and (**b**) variation of storage and loss modulus (G' and G'') as a function of time for MME mud sample.

Table 6
The influence of NaCl and $CaCl_2$ contaminations on rheological and fluid loss behavior of MME mud.

	Salt content, wt%	AV, cP	PV, cP	YP, lb/100 ft^2	YP/PV	GS (10 s/10 m), lb/100 ft^2	FL, mL
NaCl	0	23	13	20	1.54	5/8	8
	1	21.5	12	19	1.58	5/8	8.4
	2	20	11	18	1.64	4/7	9.2
	3	19	10	18	1.80	3/7	10.4
$CaCl_2$	0	23	13	20	1.54	5/8	8
	1	21	12	18	1.50	4/8	9.4
	2	19	10	18	1.80	4/6	10.2
	3	17.5	9	17	1.89	3/6	11.3

(Gautam et al., 2025). It is further observed that the YP/PV ratio of the MME mud varied in the range of 1 and 2, indicating the stability of the emulsion at high salinity conditions.

Barite sag experiments were conducted to ascertain the suspension properties of the MME mud formulation. Once the mud samples have been aged for 16 h at 120 °C, the measurement of barite sagging is carried out in a static environment. A mud sample is regarded to have an appropriate suspension when its sag factor is between 0.50 and 0.53, whereas it is deemed to have insufficient suspension characteristics if the sag factor is higher than 0.53 (Ofei et al., 2019). The measured densities at the top and bottom levels of the aging cell are shown in Table 7. The findings indicate that the sag factor of the mud samples (MME & diesel oil) falls between 0.50 and 0.53, which is considered acceptable. These findings support the hypothesis that the formulated MME mud is stable and capable of suspending cuttings at elevated temperatures.

3.2.6. Lubricity and cutting carrying efficiency

Minimizing friction between the drilling string and the wellbore is one of the essential functions of drilling mud (Caenn et al., 2011). Typically, for horizontal and directional wells, the drilling string and the wellbore remain in constant contact, and thus, it is essential to formulate a drilling fluid with adequate lubricating properties. The frictional resistance encountered during drill string rotation is referred to as torque, whereas it is referred to as drag during the hoisting and lowering of the drill string. To evaluate the performance of the formulated mud system in controlling the friction, formulated drilling fluid samples, i.e., MME and diesel mud (Table 2), along with a water-based mud comprising all additives mentioned in Table 2, except oil and SLS, were evaluated for lubricity. The CoF value of MME mud was found to be 0.14, whereas that of diesel mud was found to be 0.18. In contrast, the CoF of water-based mud was found to be 0.21. A smaller value of CoF indicates improved lubricating properties of the drilling muds. The superior lubricity of the MME mud is attributed to the adhesion of the methyl ester molecules with the metallic surface, resulting in the formation of a lubricating boundary layer (Dai et al., 2024).

The capability of drilling mud to carry drilled cuttings in the hole is estimated by its cutting carrying index (CCI) as per API recommended practice (API RP 13D, 2017). It is mentioned that a suitable hole cleaning is indicated by a CCI value more than or equal to unity, whereas an inadequate hole cleaning is revealed by a CCI value equal to or below 0.5 (API RP 13D, 2017). The CCI value was calculated using Eqs. (5)–(7), respectively, and the estimated n, K, and CCI values are presented in Table 8. Typically, CCI is predicted in the annular fluid velocity range of 51.2–153.7 ft/min (Maghrabi et al., 2020). Therefore, in this study, the CCI is calculated at 150 ft/min. Based on the calculation, the CCI of MME and

Table 7
The comparison of static sag factors of MME and diesel mud.

	MME mud	Diesel mud
ρ_{top}	1.16	1.14
ρ_{bottom}	1.21	1.22
$(\text{Sag Factor})_{Static}$	0.511	0.517

Table 8
CCI of the formulated MME and diesel mud.

Sample	θ_{600}	θ_{300}	PV	YP	n	K	CCI
MME mud	46	33	13	20	0.4792	849.41	3.185
Diesel mud	39	28	11	17	0.4781	725.77	2.722

diesel-based mud are estimated to be 3.185 and 2.722, respectively. A higher CCI value indicates a better hole-cleaning capability of MME mud.

3.2.7. Zeta potential study

The zeta potential is a measure of the difference in electrical potential between the dispersion medium and the stationary layer surrounding a dispersed particle and significantly affects the stability of the emulsion. It is mentioned that a high value of zeta potential (positive or negative) signifies the repelling of particles due to strong electrostatic forces, thus preventing aggregation or coalescence, leading to a stable emulsion (Li et al., 2023). Several studies (Avranas et al., 1988; Kumar et al., 2020a) have utilized the zeta potential to characterize the stability of oil-in-water (O/W) emulsions. For the mud samples (Table 2), the zeta potential of MME and diesel mud was found to be 38.5±0.4 and 39.4±0.5 mV, respectively. It is mentioned that a stable emulsion is indicated by a zeta potential value larger than ±30 mV, indicating the MME mud to be adequately stable in comparison to diesel oil-based emulsion mud.

The effect of polymers (XG, PAC, and CMC) on the colloidal stability of MME mud was studied by varying the concentration from 0.3 to 0.7 wt%, as shown in Fig. 10(a). It is observed that the zeta potential of the mud system increased with the polymer up to a certain concentration. The behavior is attributed to the adsorption of the negative charges present in the polymer onto the surface of emulsion droplets, causing a strong electrostatic repulsion between the droplets, thus increasing the absolute values of zeta potential (Wang et al., 2021). However, it is observed that the XG polymer reached a minimum value of 0.6 wt%, whereas CMC and PAC both showed plateau-like behavior in the 0.6–0.7 wt% regime. The above behavior is attributed to the phenomenon of polymer bridging, which leads to enhanced particle interconnectivity. Thus, the effective charge of each particle is reduced by sharing polymer chains across multiple surfaces, resulting in a decrease in the magnitude of zeta potential (Gregory and Barany, 2011). Additionally, the zeta potential of the aged (hot rolled) mud samples was evaluated after aging for 16 h at 120 °C (shown in Fig. 10(b)). From Fig. 10(b), a marginal reduction in zeta potential values was observed, indicating that the formulated MME mud samples remained unaffected, with enhanced colloidal stability at downhole conditions.

3.3. Rock-fluid interaction

3.3.1. Shale dispersion test

The effect of the interaction of formulated MME and diesel-based mud (Table 2) and cutting samples was evaluated by the shale dispersion test. The details of the weight obtained after the shale dispersion test and re-run test, and estimated primary (R_1) and secondary shale recovery (R_2) for both the MME and diesel-based mud are present in Table 9. Additionally, the shale dispersion test was performed with deionized water to determine the maximum possible dispersion tendency of the shale; the details of primary shale recovery (R_1) using deionized water are also presented in Table 9.

From Table 9, it is observed that the primary recovery of the shale samples treated with deionized water is 47.63%, while the primary recoveries of MME and diesel mud were found to be 91.50% and 86.82%, respectively. The deionized water acts as a neutral and unbuffered medium with zero ionic strength, offering no suppression of clay (kaolinite) surface charges, leading to disaggregation of shale particles. Additionally, the non-inhibition

Table 9
The weight of shale samples and estimated primary and secondary after the shale dispersion test and re-run test.

Parameter	Pure water	MME mud	Diesel mud
W_o, g	150.00	150.00	150.00
W_1, g	71.45	137.25	130.23
W_2, g	–	133.81	122.23
R_1	47.63	91.50	86.82
R_2	–	89.20	81.48

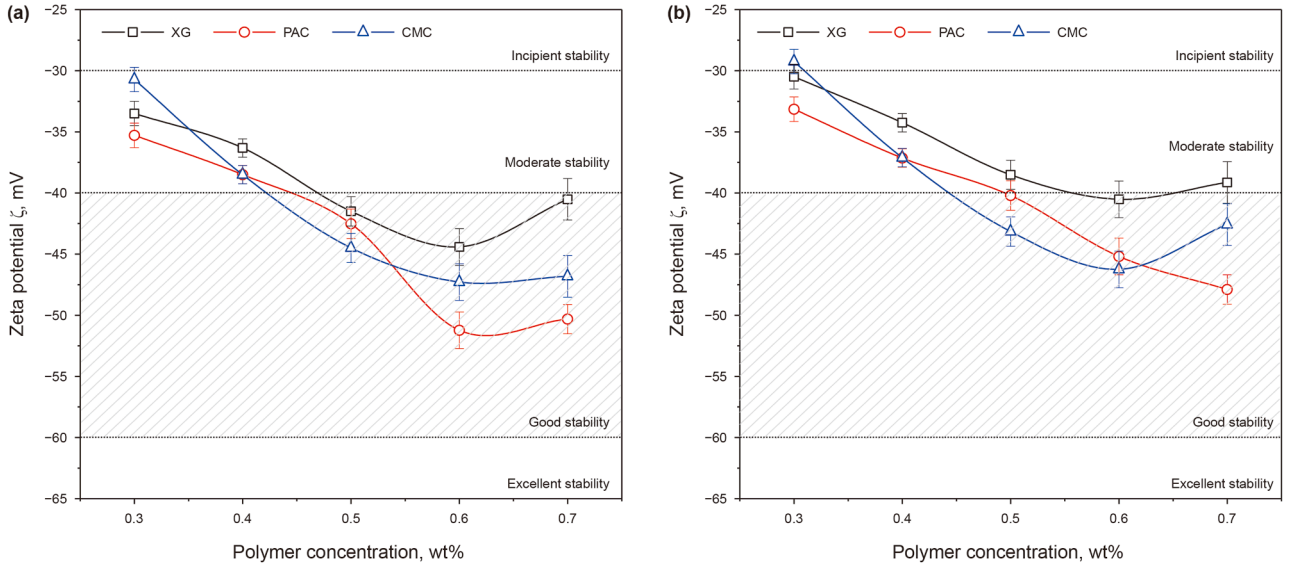

Fig. 10. The effect of polymer loading on zeta potential of MME mud at (**a**) ambient conditions and (**b**) after hot rolling at 120 °C for 16 h.

of surface charge leads to enhanced delamination of muscovite. Therefore, this results in the maximum possible shale dispersion, shown by the lowest primary recovery ratio. In contrast, both MME and diesel-based O/W emulsion mud comprise a dispersed oil phase that gets adsorbed onto the shale surface, forming a hydrophobic barrier, resulting in reduced water diffusion and mechanical erosion of the shale matrix, thereby enhancing shale stability and improving primary recovery. Furthermore, it is reported that the dispersion of cutting into the mud is the function of mud viscosity, shale compaction, testing temperature, time, and speed of rolling, and surface area of exposed cutting samples (Al-Awad and Smart, 1996). The higher viscosity of MME mud (Fig. 4(b)) provides a better cushioning effect, resulting in mechanical protection of shale samples against abrasion and cutting disintegration and, thus, further resulting in improved primary recovery, indicating enhanced inhibition to the dispersion of shale cuttings (Khodja et al., 2010). The higher recovery ratio of the rerun test shows the adherence of the hydrophobic barrier formed by MME on the shale surface, highlighting the effective shale inhibition under repeated cycles of hydration and drying or resuspension.

3.3.2. Slake durability test

A slake durability test was performed to study the weakening and disintegration of the cuttings arising from a regular drying and wetting cycle of formulated drilling fluid. The details of experimental calculations are shown in Table 10. Based on experimental data, the slake durability index (I_d) in the case of MME mud and diesel oil mud was measured to be 86.15% and 82.81%, respectively. The above results ascertain that the shale sample had outstanding inhibitive properties in MME mud. This behavior of the MME mud is attributed to the adsorption of MME molecules onto shale surfaces, resulting in the formation of a protective film-like barrier that limits water invasion, thereby contributing to the improved shale inhibition. The behavior has been hypothesized by several studies (Franklin and Chandra, 1972; Paswan et al., 2022).

3.3.3. Return permeability test

A crucial component of assessing drilling fluid performance is the return permeability test, as it provides insights into potential formation damage, hole cleaning efficiency, the performance of drilling mud, and overall wellbore stability. In the present study, the filter cake was not mechanically removed prior to the return flow stage. However, it was assumed to have been cleaned during the return flow process, as the outlet connections of the core holder allowed the passage of settled clay particles and fines. This assumption is supported by the recorded dynamic pressure data, which showed higher values at the start of the return flow period and gradually stabilized at a constant lower pressure. This trend indicates that the filter cake was progressively removed, and a steady-state flow condition was achieved after cleanup. The details of differential pressure and estimated permeability for initial and return flow for MME and diesel mud systems using the return permeability test are shown in Table 11.

Based on the experimental results, the MME mud exhibited a higher return permeability (90.18%) compared to diesel mud (78.64%). A reduction in return permeability is generally indicative of higher formation damage, which arises from the invasion of filtrate into the pore network of the reservoir rock, leading to pore blockage through mechanisms such as clay swelling, dispersion, and fines migration (Li et al., 2014).

The superior return permeability of MME mud is attributed to the polar nature of the oxygen-linked ester functional groups. The polar oxygen-linked ester groups in mahua methyl ester (MME) impart higher polarity and enable stronger dipole-dipole and hydrogen-bond interactions with water molecules, thereby lowering oil-water interfacial tension of MME as compared with diesel O/W emulsion (Supplementary Information, Section S3: 28±2 mN/m for methyl esters vs. 33±2 mN/m for diesel at 24 °C). The lower IFT values are an indication of superior emulsion stability, since reduced interfacial tension promotes finer droplet dispersion and increases the energy barrier to droplet coalescence, resulting in more stable and uniform oil-in-water emulsions (Tian et al., 2022). Additionally, a static emulsion stability test was conducted further to confirm the superior emulsion stability of MME over diesel. The details of the static emulsion stability test are mentioned in Section S4 of the Supplementary Information. The MME-based emulsion showed no visible phase separation after 24 h, whereas the diesel-based mud exhibited clear free-water separation within the same period. These results indicate higher emulsion stability of the MME O/W emulsion compared to the diesel O/W emulsion. The findings are consistent with the fundamental difference in intermolecular interactions, i.e., the polar oxygen-linked ester groups in MME (Knothe, 2005) promote stronger dipole–dipole interactions, leading to higher emulsion stability. In contrast, the non-polar hydrocarbon chains of diesel interact mainly through weak van der Waals forces (Sarıkoç, 2020), leading to reduced emulsion stability and higher free water separation.

The improved interfacial stability of MME also minimizes free-water release. It reduces filtrate loss during the API filtration test,

Table 10
The weight of shale samples and the estimated slake durability index.

Parameter	MME mud	Diesel mud
W_D, g	2500	2500
W_I, g	2825	2820
W_F, g	2780	2765
I_d	86.15	82.81

Table 11
Return permeability of MME and Diesel mud.

	MME mud				Diesel mud			
	Initial flow		Return flow		Initial flow		Return flow	
Q, cm^3/s	Differential pressure, psi	Calculated K_i, mD	Differential pressure, psi	Calculated K_f, mD	Differential pressure, psi	Calculated K_i, mD	Differential pressure, psi	Calculated K_f, mD
5.7	11.2	160.55	11.9	159.13	11.2	160.55	13.5	133.197
6.0	11.1	170.52	12.1	155.15	11.1	170.52	13.6	139.176
6.2	11.5	170.01	12.5	156.47	11.5	170.01	14.3	136.775
6.5	11.3	181.41	13.1	157.73	11.3	181.41	14.8	138.549
6.6	11.3	184.28	13.3	154.23	11.3	184.28	15.7	132.616
		Average: 173.35		Average: 156.34		Average: 173.35		Average: 136.06
	Return permeability (R_k) = 90.18%				Return permeability (R_k) = 78.64%			

as reflected by the lower API filtration volume. The enhanced emulsion integrity supports the formation of a thinner filter cake (Fig. 4(b)), facilitating more efficient cleanup during flowback. Consequently, the return permeability of cores exposed to MME mud remains higher, indicating less pore plugging and limited filtrate invasion into the porous sandstone matrix. In contrast, a thicker filter cake and higher filtration volume in diesel mud (Fig. 4(b)) lead to deeper filtrate invasion, increased interaction with clay minerals such as kaolinite and muscovite (Section 2.6.3). This increased interaction promotes dispersion and fine migration of clay minerals, leading to pore throat plugging and reduced permeability (Iscan et al., 2007).

3.4. Environmental performance and cost analysis

To evaluate the environmental impact of MME, a 96-h LC_{50} test was performed on the locally sourced shrimp (*Palaemonetes paludosus*) and compared with diesel. The percentage mortality of the test shrimp as a function of MME and diesel concentration over the 96-h exposure period is shown in Fig. 11. The LC_{50} for MME was found to be approximately 56,850 mg·L^{-1}, whereas the LC_{50} of diesel was 700 mg·L^{-1}, indicating that MME is significantly less toxic than diesel. Moreover, the LC_{50} values of MME is higher than the prescribed limit of 30,000 by the US Environmental Protection Agency (Bleier, 1991), further confirming the environmental acceptability.

The aromatic content is a critical parameter that is regulated to reduce environmental and health hazards associated with the use of OBMs and SBMs in drilling operations. The aromatic hydrocarbons have been reported to be highly toxic and prone to prolonged bioaccumulation (Neff et al., 2000). Therefore, it is pertinent to detect the presence of aromatic components in synthetic base fluids for environmental acceptability. In this regard, the presence of aromatic content was detected using ^{1}H-Nuclear Magnetic Resonance (NMR) spectroscopy (Make: Bruker, Model: AV 400). The ^{1}H-NMR spectra of MME and diesel are presented in Fig. S3 (Supplementary Information). It was observed that a set of multiplet peaks corresponding to aromatic protons appears at chemical shifts of δ = 6.0 and 9.0 ppm for diesel (Portela et al., 2016). In contrast, these peaks were absent in the synthesized MME, confirming the absence of aromatic components in MME.

To ascertain the economic feasibility of MME for drilling applications, the cost of the production of MME was estimated based on the cost of materials (crude mahua oil, methanol, and potassium hydroxide), manufacturing, and operating costs (Acevedo et al., 2015; Sudalai et al., 2023). The details of materials, manufacturing, and operating costs to produce MME are presented in Table 12. Based on cost analysis (Table 12), the cost of MME was found to be 0.4636 $/L, which is significantly lower than the cost of conventional diesel fuel (0.918 $/L in the USA).

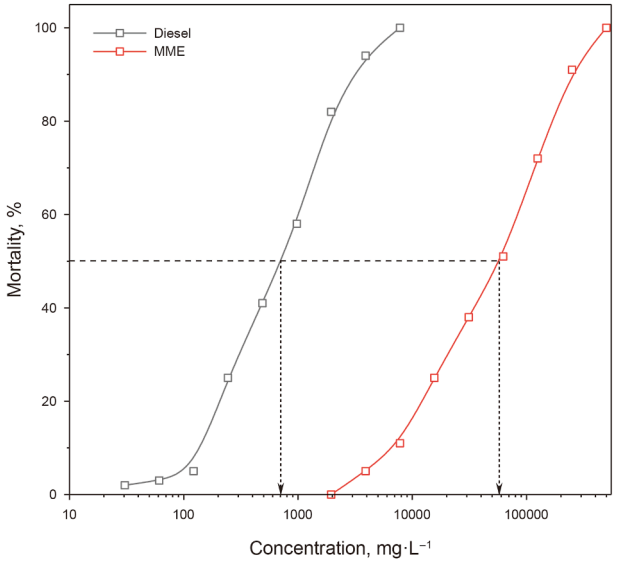

Fig. 11. The mortality (%) vs. concentration plot to estimate 96-h LC_{50} for locally sourced shrimp.

3.5. Limitations and future research directions

The present study deals with the development of MME based drilling fluid for drilling unconventional reservoirs. The formulated MME mud shows promising results in terms of thermal stability, cutting lifting capacity, shale inhibition ability, and environmental compliance. However, the limitations of the study are as follows: (i) field-scale validation of MME mud, (ii) a comprehensive performance evaluation of MME against commercially available synthetic oils for possible applications in offshore drilling operations, and (iii) advanced microstructure analysis to provide deeper mechanistic insights into the functioning of MME.

4. Conclusions

In this study, an alternative to diesel oil is developed by using mahua oil methyl ester (MME) derived from mahua oil (vegetable oil). The developed MME was used as a dispersed phase in formulating O/W emulsion mud (i.e., MME mud) and was compared with traditional diesel oil-based mud. Based on the study conducted, the following conclusions can be drawn:

- MME mud exhibited improved rheology, enhanced filtration control, and better lubricity and thermal stability compared to diesel mud. The superior performance was attributed to the formation of long-chain fatty acid methyl ester (FAME) molecules containing both hydrophobic alkyl chains and polar ester functionalities.

Table 12
Material, manufacturing, and operating costs to produce MME.

Cost component	Unit	Price	Material required to produce 1 L of biodiesel (yield = 89.1%)	Cost contribution, $/L
Materials				
Crude mahua oil	$/L	0.3108	1.029 L	0.3198
Methanol	$/L	0.2930	0.264 L	0.0774
Potassium hydroxide	$/kg	0.6000	0.0052 kg	0.0031
Manufacturing (labor and electricity)	$/L	0.0423		0.0423
Operating cost (quality analysis and maintenance)	$/L	0.0211		0.0211
Total cost				**0.4636**

- The viscoelastic studies of MME mud revealed a stable gel-like structure essential for suspending drill cuttings under both prolonged static and repeated mechanical stress conditions.
- The MME mud showed improved shale stability resulting from the adsorption of FAME molecules onto shale surfaces, which formed a protective film-like barrier to limit water invasion.
- The MME mud exhibited higher return permeability than diesel mud, attributed to the stronger dipole-dipole interaction among the ester functional groups. These interactions improve emulsion stability, reduce free water separation, and minimize filtrate invasion.
- MME was found to be free of aromatic hydrocarbons and exhibited a higher LC_{50}, thereby reducing the risk of bioaccumulation and toxicity. Additionally, the cost analysis showed that MME is more economical than diesel oil.

The above findings confirm that MME can be a suitable alternative to diesel oil for formulating emulsion-based drilling fluid, especially in: (i) shale-prone formations, where inhibition of clay swelling and dispersion is essential; (ii) directional and extended-reach wells, where enhanced lubricity is required to minimize torque, drag, and stuck-pipe risks; (iii) environmentally sensitive areas, where reduced ecotoxicity relative to diesel is both a regulatory and operational priority; and (iv) economically sensitive drilling zones, where MME offers a cost-effective balance by matching the performance of diesel OBMs while providing a significantly lower environmental footprint.

CRediT authorship contribution statement

Bhola Kumar Paswan: Writing – original draft, Validation, Methodology, Investigation, Formal analysis, Conceptualization. **Smruti Naik:** Visualization, Software, Formal analysis, Data curation. **Puja Hansdah:** Validation, Project administration, Formal analysis. **Sidharth Gautam:** Writing – review & editing, Writing – original draft, Validation, Supervision, Methodology, Investigation.

Declaration of interests

The authors declare that they have no known competing financial interests or personal relationships that could have appeared to influence the work reported in this paper.

Acknowledgements

The authors (**BKP & SN**) would like to acknowledge Parul University, Vadodara, Gujarat, and the Indian Institute of Technology, Delhi, for providing financial assistance and necessary laboratory facilities for this work. The author (**SG**) acknowledges the financial and laboratory support provided by the Rajiv Gandhi Institute of Petroleum Technology, Jais, through Seed Grant (SG-2301). The financial support provided by the Anusandhan National Research Foundation (ANRF) through the project grant (EEQ/2023/000331) is also sincerely acknowledged.

Appendix A. Supplementary data

Supplementary data to this article can be found online at https://doi.org/10.1016/j.petsci.2025.12.019.

References

Abdo, J., Haneef, M.D., 2012. Nano-enhanced drilling fluids: pioneering approach to overcome uncompromising drilling problems. J. Energy Resour. Technol. 134 (1), 1–7. https://doi.org/10.1115/1.4005244.

Abed, M.A., Rasaei, M.R., 2024. Experimental study of hydrophilic additives on filter cake permeability and filtrate losses. Can. J. Chem. Eng. 102 (5), 1825–1841. https://doi.org/10.1002/cjce.25167.

Aboulrous, A.A., Haddad, A.S., Rafati, R., Boyou, N.V., Alsabagh, A.M., 2022. Review of synthesis, characteristics and technical challenges of biodiesel based drilling fluids. J. Clean. Prod. 336, 130344. https://doi.org/10.1016/j.jclepro.2021.130344.

Acevedo, J.C., Hernández, J.A., Valdés, C.F., Khanal, S.K., 2015. Analysis of operating costs for producing biodiesel from palm oil at pilot-scale in Colombia. Bioresour. Technol. 188, 117–123. https://doi.org/10.1016/j.biortech.2015.01.071.

Adams, N., Charrier, T., 1985. Drilling Engineering: A Complete Well Planning Approach. Pennwell Corporation.

Adewale, D., Ogunrinde, J.O., 2010. Development of environmentally friendly oil based mud using palm- oil and groundnut-oil. In: Nigeria Annual International Conference and Exhibition, pp. 934–942. https://doi.org/10.2118/140720-MS.

Agwu, O.E., Okon, A.N., Udoh, F.D., 2015. A comparative study of diesel oil and soybean oil as oil-based drilling mud. J. Pet. Eng. 1–10. https://doi.org/10.1155/2015/828451.

Ahmed, A., Elkatatny, S., Al-Afnan, S., 2021. Applications of biodiesel in drilling fluids. Geofluids 1–11. https://doi.org/10.1155/2021/5565897.

Al-Awad, M.N.J., Smart, B.G.D., 1996. Characterization of shale-drilling fluid interaction mechanisms related to wellbore instability. J. King Saud Univ. Eng. Sci. 8 (2), 187–214. https://doi.org/10.1016/S1018-3639(18)30657-3.

Amanullah, M., 2005. Physio-chemical characterisation of vegetable oils and preliminary test results of vegetable oil-based muds. In: Proceedings of SPE/IADC Middle East Drilling Technology Conference and Exhibition, pp. 95–103. https://doi.org/10.2523/97008-MS.

API RP 13B-2, 2019. In: Recommended Practice for Field Testing Oil-based Drilling Fluids, fifth ed. American Petroleum Institute.

API RP 13D, 2017. In: Recommended Practice on the Rheology and Hydraulics of oil-well Drilling Fluids, seventh ed. American Petroleum Institute.

API RP 13I, 2023. In: Recommended Practice for Laboratory Testing of Drilling Fluids, ninth ed. American Petroleum Institute.

Arain, A.H., Ridha, S., Ali, I., 2023. Development and performance evaluation of castor oil based biodiesel as an eco-friendly ester-based drilling fluid. Pet. Sci. Technol. 41 (19), 1831–1851. https://doi.org/10.1080/10916466.2022.2097260.

Arain, A.H., Ridha, S., Suppiah, R.R., Irawan, S., Ilyas, S.U., 2022. Developing an efficient ester-based drilling fluid based on Calophyllum Inophyllum oil for eco-friendly drilling of unconventional shale formation. J. Pet. Sci. Eng. 219, 111141. https://doi.org/10.1016/j.petrol.2022.111141.

ASME, 2005. Drilling Fluids Processing Handbook. Elsevier. https://doi.org/10.1016/B978-0-7506-7775-2.X5000-8.

ASTM D975, 2021. Specification for Diesel Fuel. https://doi.org/10.1520/D0975-21.

Atkins, P., de Paula, J., Keeler, J., 2023. In: Atkins' Physical Chemistry, eleventh ed. Oxford University Press.

Avranas, A., Stalidis, G., Ritzoulis, G., 1988. Demulsification rate and zeta potential of O/W emulsions. Colloid Polym. Sci. 266 (10), 937–940. https://doi.org/10.1007/BF01410850.

Bai, M.T., Swarna, U., Raju, C.A.I., Sridevi, V., 2021. Production of methyl ester from mahua oil: characterization and optimization by using RSM. Mater. Today Proc. 44, 1609–1616. https://doi.org/10.1016/j.matpr.2020.11.815.

Baxter, R., Offenbacher, M., Bedel, D., Lemaire, P., Miano, C., 2018. Transitions from diesel muds: options, properties, and a proposal. In: AADE Fluids Technical Conference and Exhibition. Texas, USA.

Bayat, A.E., Harati, S., Kolivandi, H., 2021. Evaluation of rheological and filtration properties of a polymeric water-based drilling mud in presence of nano additives at various temperatures. Coll. Surf. A Physicochem. Eng. Asp. 627, 127128. https://doi.org/10.1016/j.colsurfa.2021.127128.

Bleier, R., 1991. Predicting mud toxicity. J. Petrol. Technol. 43 (10), 1192–1193. https://doi.org/10.2118/23572-PA.

Bui, B., Saasen, A., Maxey, J., Ozbayoglu, M., 2012. Viscoelastic properties of oil-based drilling fluids. In: Annual Transactions of the Nordic Rheology Society, pp. 33–47.

Caenn, R., Chillingar, G.V., 1996. Drilling fluids: State of the art. J. Pet. Sci. Eng. 14 (3–4), 221–230. https://doi.org/10.1016/0920-4105(95)00051-8.

Caenn, R., Darley, H.C.H., Gray, G.R., 2011. Composition and Properties of Drilling and Completion Fluids. Gulf Professional Publishing. https://doi.org/10.1016/C2015-0-04159-4.

Chen, H., Kuru, E., Hu, K., 2023. A generalized model for field assessment of particle settling velocity in aviscoelastic fluid. Powder Technol. 427, 118697. https://doi.org/10.1016/j.powtec.2023.118697.

Cheraghian, G., 2017. Application of nano-particles of clay to improve drilling fluid. Int. J. Nanosci. Nanotechnol. 13 (2), 177–186.

Chilingarian, G.V., Alp, E., Caenn, R., Al-Salem, M., Uslu, S., Gonzales, S., Dorovi, R.J., Mathur, R.M., Yen, T.F., 1986. Drilling fluid evaluation using yield point-plastic viscosity correlation. Energy Sources 8 (2–3), 233–244. https://doi.org/10.1080/00908318608946052.

Dai, Y., Lu, F., Tang, Y., Wang, Y., He, X., Wang, T., Wu, J., 2024. The simulation of ester lubricants and their application in weak gel drilling fluids. Gels 10 (3), 178. https://doi.org/10.3390/gels10030178.

Edalatfar, M., Yazdani, F., Salehi, M.B., 2021. Synthesis and identification of ZnTiO3 nanoparticles as a rheology modifier additive in water-based drilling mud. J. Pet. Sci. Eng. 201, 108415. https://doi.org/10.1016/j.petrol.2021.108415.

Fadairo, A., Adeyemi, G., Ogunkunle, T., Ling, K., Rasouli, V., Effiong, E., Ayoo, J., 2021. Study the suitability of neem seed oil for formulation of eco-friendly oil

based drilling fluid. Pet. Res. 6 (3), 283–290. https://doi.org/10.1016/j.ptlrs.2021.02.003.
Fakoya, M.F., Ahmed, R.M., 2018. A generalized model for apparent viscosity of oil-based muds. J. Pet. Sci. Eng. 165, 777–785. https://doi.org/10.1016/j.petrol.2018.03.029.
Fox, N.J., Stachowiak, G.W., 2007. Vegetable oil-based lubricants-a review of oxidation. Tribol. Int. 40 (7), 1035–1046. https://doi.org/10.1016/j.triboint.2006.10.001.
Franklin, J.A., Chandra, R., 1972. The slake-durability test. Int. J. Rock Mech. Min. Sci. Geomech. Abstr. 9 (3), 325–328. https://doi.org/10.1016/0148-9062(72)90001-0.
Gautam, S., Guria, C., 2022. An improved prediction of frictional pressure drop using an accurate shear rate equation for high-yield stress drilling fluids at the surface and downhole conditions. J. Pet. Sci. Eng. 218, 110981. https://doi.org/10.1016/j.petrol.2022.110981.
Gautam, S., Guria, C., 2020. Optimal synthesis, characterization, and performance evaluation of high-pressure high-temperature polymer-based drilling fluid: The effect of viscoelasticity on cutting transport, filtration loss, and lubricity. SPE J. 25 (3), 1333–1350. https://doi.org/10.2118/200487-PA.
Gautam, S., Kumar, S., Kumar, A., Rajak, V.K., Guria, C., 2025. Development of functional polymer-based clay-free HPHT drilling fluid: Effect of molecular weight and its distribution on drilling fluid performance. Geoenergy Sci. Eng. 246, 213616. https://doi.org/10.1016/j.geoen.2024.213616.
Gregory, J., Barany, S., 2011. Adsorption and flocculation by polymers and polymer mixtures. Adv. Colloid Interface Sci. 169 (1), 1–12. https://doi.org/10.1016/j.cis.2011.06.004.
Guo, H., Brûlet, A., Rajamohanan, P.R., Marcellan, A., Sanson, N., Hourdet, D., 2015. Influence of topology of LCST-based graft copolymers on responsive assembling in aqueous media. Polymer 60, 164–175. https://doi.org/10.1016/j.polymer.2015.01.038.
Iscan, A.G., Civan, F., Kok, M.V., 2007. Alteration of permeability by drilling fluid invasion and flow reversal. J. Pet. Sci. Eng. 58 (1–2), 227–244. https://doi.org/10.1016/j.petrol.2007.01.002.
Jiang, G., Shi, H., He, Y., 2022. The biodiesel-based flat-rheology drilling fluid system. Petrol. Explor. Dev. 49 (1), 173–182. https://doi.org/10.11698/PED.2022.01.16.
Kania, D., Yunus, R., Omar, R., Abdul Rashid, S., Mohamed Jan, B., 2021. Rheological investigation of synthetic-based drilling fluid containing non-ionic surfactant pentaerythritol ester using full factorial design. Coll. Surf. A Physicochem. Eng. Asp. 625, 126700. https://doi.org/10.1016/j.colsurfa.2021.126700.
Khodja, Mohamed, Canselier, J.P., Bergaya, F., Fourar, K., Khodja, Malika, Cohaut, N., Benmounah, A., 2010. Shale problems and water-based drilling fluid optimisation in the Hassi Messaoud Algerian oil field. Appl. Clay Sci. 49 (4), 383–393. https://doi.org/10.1016/j.clay.2010.06.008.
Knothe, G., 2005. Dependence of biodiesel fuel properties on the structure of fatty acid alkyl esters. Fuel Process. Technol. 86 (10), 1059–1070. https://doi.org/10.1016/j.fuproc.2004.11.002.
Kumar, N., Ali, S., Kumar, A., Mandal, A., 2020a. Design and formulation of surfactant stabilized O/W emulsion for application in enhanced oil recovery: Effect of pH, salinity and temperature. Oil Gas Sci. Technol. 75, 72. https://doi.org/10.2516/ogst/2020066.
Kumar, S., Thakur, A., Kumar, N., Husein, M.M., 2020b. A novel oil-in-water drilling mud formulated with extracts from Indian mango seed oil. Pet. Sci. 17, 196–210. https://doi.org/10.1007/s12182-019-00371-7.
Li, A., Gao, S., Zhang, G., Zeng, Y., Hu, Y., Zhai, R., Dong, A., Zhang, J., 2024. A review in polymers for fluid loss control in drilling operations. Macromol. Chem. Phys. 225 (8), 2300390. https://doi.org/10.1002/macp.202300390.
Li, D., Leonard, R., He, W., 2014. Deciphering return permeabilities. In: SPE International Symposium and Exhibition on Formation Damage Control. https://doi.org/10.2118/168119-MS.
Li, K., Zhong, W., Li, P., Ren, J., Jiang, K., Wu, W., 2023. Antibacterial mechanism of lignin and lignin-based antimicrobial materials in different fields. Int. J. Biol. Macromol. 252, 126281. https://doi.org/10.1016/j.ijbiomac.2023.126281.
Li, M.C., Wu, Q., Song, K., De Hoop, C.F., Lee, S., Qing, Y., Wu, Y., 2016a. Cellulose nanocrystals and polyanionic cellulose as additives in bentonite water-based drilling fluids: rheological modeling and filtration mechanisms. Ind. Eng. Chem. Res. 55 (1), 133–143. https://doi.org/10.1021/acs.iecr.5b03510.
Li, W., Zhao, X., Ji, Y., Peng, H., Li, Y., Liu, L., Han, X., 2016b. An investigation on environmentally friendly biodiesel-based invert emulsion drilling fluid. J. Pet. Explor. Prod. Technol. 6 (3), 505–517. https://doi.org/10.1007/s13202-015-0205-7.
Liu, L., Pu, X., Zhou, Y., Wu, X., Luo, D., Ren, Z., 2020. Phase inversion of pickering emulsions by electrolyte for potential reversible water-in-oil drilling fluids. Energy Fuels 34 (2), 1317–1328. https://doi.org/10.1021/acs.energyfuels.9b03117.
Lysakova, E.I., Skorobogatova, A.D., Shashkova, T.L., Grigoriev, Y.S., Neverov, A.L., Pryazhnikov, M.I., 2025. Environmentally friendly technical plant oils as the base for emulsion drilling fluids. Emergent Mater 8 (3), 2307–2324. https://doi.org/10.1007/s42247-024-00944-2.
Maghrabi, S.S., Waggy, P., Engel, A.S., Sisson, T., 2020. Low ECD, sag-resistant, non-damaging, barite-free invert emulsion reservoir drill-in fluid comprising novel weighting, emulsifier and filtration control additives. In: AADE Fluids Technical Conference and Exhibition. Houston, Texas, USA.
Melton, H.R., Smith, J.P., Martin, C.R., Nedwed, T.J., Mairs, H.L., Raught, D.L., 2000. Offshore discharge of drilling fluids and cuttings- A scientific perspective on public policy. In: Rio Oil & Gas Expo Conference, pp. 1–13.
Mezger, T.G., 2006. The Rheology Handbook: for Users of Rotational and Oscillatory Rheometers, KG. Vincentz Network GmbH & Co.
Neff, J.M., McKelvie, S., Ayers, R.C.J., 2000. Environmental impacts of synthetic based drilling fluids. Report Prepared for Minerals Management Service (MMS). Robert Ayers & Associates.
Ofei, T.N., Saasen, A., Lund, B., Sangesland, S., Gyland, K., Harald, L., 2019. A new approach to dynamic barite sag analysis on typical field oil-based drilling fluid. Annu. Trans. Nord. Rheol. Soc. 27, 61–69.
Olaniyan, D.D., Sarah, A.A., 2024. The rheological and filtration properties of black seed (Nigella Sativa L.) ester as a base fluid in drilling fluid. J. Eng. Appl. Sci. 71 (1), 17. https://doi.org/10.1186/s44147-023-00352-z.
Paswan, B.K., Kumar, S., Mahto, V., 2022. Evaluation of a soybean oil derived surfactant in the development of oil-in-water (O/W) emulsion drilling mud for shale formation. J. Pet. Sci. Eng. 217, 110926. https://doi.org/10.1016/j.petrol.2022.110926.
Paswan, B.K., Mahto, V., 2020. Development of environment-friendly oil-in-water emulsion based drilling fluid for shale gas formation using sunflower oil. J. Pet. Sci. Eng. 191, 107129. https://doi.org/10.1016/j.petrol.2020.107129.
Portela, N.A., Oliveira, E.C.S., Neto, A.C., Rodrigues, R.R.T., Silva, S.R.C., Castro, E.V.R., Filgueiras, P.R., 2016. Quantification of biodiesel in petroleum diesel by ^{1}H NMR: Evaluation of univariate and multivariate approaches. Fuel 166, 12–18. https://doi.org/10.1016/j.fuel.2015.10.091.
Power, D., Zamora, M., 2003. Drilling fluid yield stress: measurement techniques for improved understanding of critical drilling fluid parameters. In: AADE Technical Conference, pp. 1–3.
Rabelo, S.N., Ferraz, V.P., Oliveira, L.S., Franca, A.S., 2015. FTIR analysis for quantification of fatty acid methyl esters in biodiesel produced by microwave-assisted transesterification. Int. J. Environ. Sustain Dev. 6 (12), 964–969. https://doi.org/10.7763/ijesd.2015.v6.730.
Ratkievicius, L.A., Cunha Filho, F.J.V. Da, Barros Neto, E.L. De, Santanna, V.C., 2017. Modification of bentonite clay by a cationic surfactant to be used as a viscosity enhancer in vegetable-oil-based drilling fluid. Appl. Clay Sci. 135, 307–312. https://doi.org/10.1016/j.clay.2016.10.011.
Razali, S.Z., Yunus, R., Abdul Rashid, S., Lim, H.N., Mohamed Jan, B., 2018. Review of biodegradable synthetic-based drilling fluid: Progression, performance and future prospect. Renew. Sustain. Energy Rev. 90, 171–186. https://doi.org/10.1016/j.rser.2018.03.014.
Sabariswaran, K., Selvakumar, Sundararaj, Kathirselvi, A., Selvakumar, S., 2014. Biodiesel production from mahua oil by using two-step trans-esterification process. Chem. Sci. Rev. Lett. 3 (9), 52–57.
Said, M.M., El-Sayed, A.A.H., 2018. The use of palm oil fatty acid methyl ester as a base fluid for a flat rheology high-performance drilling fluid. J. Pet. Sci. Eng. 166, 969–983. https://doi.org/10.1016/j.petrol.2018.03.101.
Saleh, T.A., Ibrahim, M.A., 2019. Advances in functionalized nanoparticles based drilling inhibitors for oil production. Energy Rep. 5, 1293–1304. https://doi.org/10.1016/j.egyr.2019.06.002.
Sarıkoç, S., 2020. Fuels of the Diesel-gasoline Engines and their Properties. In: Diesel and Gasoline Engines. https://doi.org/10.5772/intechopen.89044.
Setyawan, W., 2018. Alternative use of castor oil for vegetable oil-based mud environmentally friendly potential domestic oil-based mud. In: Proc. Indon Petrol. Assoc., 35th Ann. Conv. https://doi.org/10.29118/IPA.278.11.E.015.
Sharma Dugala, N., Singh Goindi, G., Sharma, A., 2021. Evaluation of physico-chemical characteristics of Mahua (*Madhuca indica*) and Jatropha (Jatropha curcas) dual biodiesel blends with diesel. J. King Saud Univ. Eng. Sci. 33 (6), 424–436. https://doi.org/10.1016/j.jksues.2020.05.006.
Singh, A., Singh, I.S., 1991. Chemical evaluation of mahua (*Madhuca indica*) seed. Food Chem. 40 (2), 221–228. https://doi.org/10.1016/0308-8146(91)90106-X.
Socrates, G., 2004. Infrared and Raman Characteristic Group Frequencies: Tables and Charts. John Wiley & Sons.
Sönmez, A., Verşan Kök, M., Özel, R., 2013. Performance analysis of drilling fluid liquid lubricants. J. Pet. Sci. Eng. 108, 64–73. https://doi.org/10.1016/j.petrol.2013.06.002.
Sudalai, S., Rupesh, K.J., Devanesan, M., Arumugam, A., 2023. A critical review of *Madhuca indica* as an efficient biodiesel producer: Towards sustainability. Renew. Sustain. Energy Rev. 188, 113811. https://doi.org/10.1016/j.rser.2023.113811.
Sulaimon, A.A., Adeyemi, B.J., Rahimi, M., 2017. Performance enhancement of selected vegetable oil as base fluid for drilling HPHT formation. J. Pet. Sci. Eng. 152, 49–59. https://doi.org/10.1016/j.petrol.2017.02.006.
Tian, Y., Zhou, J., He, C., He, L., Li, X., Sui, H., 2022. The formation, stabilization and separation of oil–water emulsions: A review. Processes 10 (4), 738. https://doi.org/10.3390/pr10040738.
Tiwari, R., Kumar, S., Husein, M.M., Rane, P.M., Kumar, N., 2020. Environmentally benign invert emulsion mud with optimized performance for shale drilling. J. Pet. Sci. Eng. 186, 106791. https://doi.org/10.1016/j.petrol.2019.106791.
Udoh, F.D., Itah, J.J., Okon, A.N., 2012. Formulation of synthetic-based drilling fluid using palm oil derived Ester. Asian J. Microbiol. Biotechnol. Environ. Sci. 14 (2), 175–180.
Wang, D., Yang, Diling, Huang, C., Huang, Y., Yang, Dingzheng, Zhang, H., Liu, Q., Tang, T., Gamal El-Din, M., Kemppi, T., Perdicakis, B., Zeng, H., 2021. Stabilization mechanism and chemical demulsification of water-in-oil and oil-in-water emulsions in petroleum industry: A review. Fuel 286, 119390. https://doi.org/10.1016/j.fuel.2020.119390.
Wei, Z., Wang, M., Li, Y., An, Y., Li, K., Bo, K., Guo, M., 2022. Sodium alginate as an eco-friendly rheology modifier and salt-tolerant fluid loss additive in water-based drilling fluids. RSC Adv. 12, 29852–29864. https://doi.org/10.1039/d2ra04448j.

Werner, B., Myrseth, V., Saasen, A., 2017. Viscoelastic properties of drilling fluids and their influence on cuttings transport. J. Pet. Sci. Eng. 156, 845–851. https://doi.org/10.1016/j.petrol.2017.06.063.

William, J.K.M., Ponmani, S., Samuel, R., Nagarajan, R., Sangwai, J.S., 2014. Effect of CuO and ZnO nanofluids in xanthan gum on thermal, electrical and high pressure rheology of water-based drilling fluids. J. Pet. Sci. Eng. 117, 15–27. https://doi.org/10.1016/j.petrol.2014.03.005.

Yonebayashi, H., Miyagawa, Y., Watanabe, T., Kurokawa, S., Teshima, S., Richmond, M.H., 2017. Return permeability tests and relevant laboratory evaluation to optimize remedial design for reviving productivity of cased hole well damaged by oil-based-mud. In: Abu Dhabi International Petroleum Exhibition & Conference, pp. 1–12. https://doi.org/10.2118/188755-MS.

Yue, Q., Ma, B., 2008. Development and applications of solids-free oil-in-water drilling fluids. Pet. Sci. 5 (2), 153–158. https://doi.org/10.1007/s12182-008-0023-3.